Molecular characterization of the type VII secretion system in *Bacillus* species

(バシルス属細菌 VII 型分泌装置の分子機能解析)

Harvey Kakoma Kamboyi

Division of Infection and Immunity

International Institute for Zoonosis Control

Graduate School of Infectious Diseases

Hokkaido University

2025

Table of contents

Abbreviations

Amp^R	Ampicillin resistance
ANOVA	Analysis of variance
BA	Blood agar
BHI	Brain-heart infusion
CFU	Colony-forming unit
CSA	Cereus selective agar
DNA	Deoxyribonucleic acid
DS	Downstream
DSM	Difco sporulation medium
GFP	Green fluorescent protein
Kan^R	Kanamycin resistance
LB	Luria-Bertani
LBGM	Luria-Bertani + glycerol + manganese
LC-MS/MS	Liquid chromatography-tandem mass spectrometry
M9	Minimal medium salts
PCR	Polymerase chain reaction
Pmx	Polymyxin B
RFP	Red fluorescent protein
Spe	Spectinomycin
Spe^R	Spectinomycin resistance
Tet^R	Tetracycline resistance
T7SS	Type VII secretion system
T7SSa	Type VIIa secretion system
T7SSb	Type VIIb secretion system
TA	Toxin-antitoxin
US	Upstream
WT	Wild type

Unit measure abbreviations

bp	base pair
Da	dalton
°C	degree celsius
g	gram
h	hour
kb	kilobase
l	litre
ml	millilitres
mm	millimetre
mM	millimolar
µF	microfarad
µg	microgram
µl	microliter
µm	micrometer
µM	micromolar
min	minute
ng	nanogram
nl	nanoliter
Ω	ohm
ppm	parts per million
%	per cent
pH	potential hydrogen
rpm	revolution per minute
vol	volume
V	volt
wt	weight

Notes

The contents of Chapters I and II have been published in BMC Microbiology, Springer Nature.

Kamboyi H.K, Paudel A, Shawa M, Sugawara M, Zorigt T, Chizimu J.Y, Kitao T, Furuta Y, Hang'ombe B.M, Munyeme M, and Higashi H. **EsxA, a type VII secretion system-dependent effector, reveals a novel function in the sporulation of *Bacillus cereus* ATCC14579**. *BMC Microbiology*, 24:351, 2024.

Preface

Of the hundreds of species in the genus *Bacillus*, the two of greatest public health importance are *B. cereus sensu stricto* (herein referred to as *B. cereus*) and *B. anthracis* [1,2]. The two are genetically closely related and classified into the same group named the *B. cereus* group, which also includes *B. thuringiensis, B. mycoides, B. pseudomycoides, B. weihenstephanensis, B. cytotoxicus* and *B. toyonensis*. This group is characterized by Gram-positive, spore-forming, aerobic, facultatively anaerobic and rod-shaped bacteria. Genomically, they possess a low guanine-cytosine content, which is characteristic of the phylum Firmicutes. The definition of these species and the distribution of the strains within them have been based on their phenotypes and clinical and economic significance [2–4].

B. cereus has long been an important cause of food poisoning in humans, causing two types of gastrointestinal illness, including emesis and diarrhoea, after consumption of contaminated food. Different toxins produced by this bacterium characterize the pathogenicity of *B. cereus* [5]. Diarrhoea is associated with a series of enterotoxins, including haemolysin BL, non-haemolytic enterotoxin, cytotoxin K and enterotoxin FM, while the emetic syndrome is caused by the toxin cereulide [6]. Recently, *B. cereus* has gained notoriety as the etiological agent for various severe extra-intestinal infections and is acquiring increasing importance as an agent of nosocomial infections [7,8]. Many virulence factors have been postulated in recent strains, and their pathogenic mechanisms are still being investigated. In veterinary medicine, *B. cereus* causes mild to severe gangrenous mastitis in cattle and goats [9], abortion and haemorrhagic disease in dromedary camels [10] and generalized fatal infections in Chinese softshell turtles [11].

One of the mechanisms by which bacteria express their pathogenicity is through specialized secretion systems, composite multi-protein structures, which are used to translocate virulence factors across membranes into the host. These virulence factors, also called effector proteins, function to invade mammalian hosts, damage tissue sites and thwart the immune system from responding [12]. Several secretion systems have been identified in bacteria and classified from I to XI [13,14], but Gram-negatives encode the majority. Gram-positives like *B. cereus* and *B. anthracis* use the type VII secretion system (T7SS), which has been extensively studied in *Mycobacterium tuberculosis* and *Staphylococcus aureus* and to a lesser extent in Group B *Streptococcus, Listeria monocytogenes*. The T7SS was first discovered in *Mycobacterium tuberculosis* [15], and recent studies on Gram-positive bacteria have shown limited homology to the mycobacterial T7SS components, which led to the sub-classification of T7SS into T7SSa

(Actinobacteria) and T7SSb (Firmicutes) [16,17]. The early secreted antigenic target type A (EsxA) and B (EsxB) are typical T7SS-dependent pore-forming toxins and T-cell antigens. Their secretion depends on the functional membrane-bound ATPase of the Ftsk/SpoIIIE family termed EssC [18–23]. EsxA and EsxB possess a conserved Trp–Xaa–Gly (WXG) central sequence motif having ~100 amino acids, from which their family name, WXG100, originates. Additionally, WXG100-like proteins, EsxC and EsxD, have been identified in *S. aureus*, and the polymorphic LXG toxin among Firmicutes and their functions have been characterized [24–26]. Among all these T7SS substrates, EsxA has been extensively studied, and its role in host-pathogen interactions is continuously being unravelled. For example, in *Mycobacterium tuberculosis*, EsxA disrupts the phagosomal membrane, facilitating the escape of bacteria from the phagosome into the host cell cytoplasm, where it can avoid degradation [19]. In *S. aureus*, EsxA has been found to induce host cell apoptosis [27] and is essential for abscess formation [28].

Studies on T7SS continue to focus on its involvement in host-immune interactions and niche adaptations. However, given the inter and intraspecies variations in the T7SS repertoire [29,30], uncovering the intrinsic roles of the T7SS is paramount. The information gathered could provide insights into the pathways they are involved in and serve as new targets for antimicrobials in the wake of emerging drug-resistant bacteria [31]. Bacterial secretion systems have now become an attractive target for developing antibacterials as they are essential in the pathogenesis of many bacteria [32–34]. However, the T7SS repertoire in *B. cereus* has not been reported yet. It is, therefore, imperative to identify the *B. cereus* T7SS and explore its biological significance in its lifecycle and infection. Meanwhile, the *B. anthracis* T7SS lacks EsxA, but its EsxB is not only a secreted effector but also indispensable for the secretion of other T7SS substrates and immunogenic in *B. anthracis*-infected guinea pigs [35].

Other than being equipped with survival mechanisms in the host, pathogenic bacteria are also well adapted to thrive in the natural environment until they infect the host [36]. *Bacillus* species have the ability to form spores to survive harsh environmental conditions such as nutrition deprivation, chemical exposure, desiccation, heat and ultraviolet radiation [37,38]. The process of spore formation, sporulation, is a highly regulated process of cellular differentiation in response to environmental stimuli [39,40]. This makes *Bacillus* species a group of versatile organisms capable of thriving in diverse environments. Thus, their pathogenesis depends upon the survival of spores in the non-host environment, as dormant spores are the main infectious form of the bacterium.

In this thesis, Chapter I describes the identification of *B. cereus* T7SS and its effector proteins, EsxA1 and EsxA2, through genomic analyses and liquid chromatography-tandem mass spectrometry (LC-MS/MS). Chapter II provides evidence that deletion of both genes encoding the two EsxA proteins affected the sporulation of *B. cereus* under sporulation-inducing conditions by assessing the influence of the identified effectors on the phenotypic characteristics of *B. cereus* ATCC14579.

CHAPTER I

Identification of type VII secretion system and its effector proteins in *Bacillus species*

Summary

The study explores the type VII secretion system (T7SS) in *Bacillus species*, a mechanism essential for bacterial virulence yet previously uncharacterized in this species. The T7SS of *Bacillus* species was analyzed, focusing on its gene cluster organization and potential for secretion of virulence factors. Comparison with *Staphylococcus aureus*, known for its well-studied T7SS, showed that *B. cereus* has a similar gene arrangement, although with low sequence homology overall, averaging below 52%. Unique to *B. cereus*, the study identified an additional T7SS-associated gene (*esxA*) and a *tigR* encoding a chaperon for the LXG toxin, suggesting specific adaptations in this bacterium's T7SS. The research also found variability in the T7SS among different *B. cereus* strains, notably downstream of the *essC* gene. Clinical isolates possessed additional virulence genes, while non-pathogenic strains did not, implying that T7SS variation may correlate with virulence. Comparative analysis with related *Bacillus* species, such as *B. subtilis* and *B. anthracis*, demonstrated distinct T7SS compositions, reinforcing the diversity of T7SS within the Firmicutes phylum. Notably, *B. anthracis* encodes two out of the five typical T7SS structural proteins and five WXG100-like proteins staggered across the genome, one of which is plasmid-encoded. In addition, *B. anthracis* also possess an *sseB* gene within the T7SS gene cluster that encodes a well-known component of the T3SS translocon and is key to the pathogenicity and virulence of pathogenic *Salmonella* species.

Functional analysis was conducted by deleting the *essC* gene in *B. cereus*, which resulted in the absence of EsxA proteins in the mutant's secretome. This finding confirmed that EssC is essential for T7SS activity and secretion of EsxA proteins. The study's discovery of two homologous EsxA proteins with 94% sequence identity, likely form homodimers, highlights a secretion mechanism distinct from other species where EsxA and EsxB heterodimers are common. These findings underscore the structural and functional diversity of T7SSs across species, emphasizing caution when generalizing T7SS roles across related bacteria.

Introduction

Bacterial secretion systems are composite multi-protein structures used to translocate macromolecules, mostly protein in nature, across membranes. The secreted proteins can promote bacterial virulence by directly intoxicating target cells and disrupting their functions. In total, 11 secretion systems have been identified and classified I–XI [13,14]. Ten secretion systems are dedicated to Gram-negative bacteria, while Gram-positives utilize the T7SS only [41,42]. The distinction between secretion types would primarily be that the secretion systems have different protein compositions and mechanisms. Further, with recent advances in research technology, there seems to be a plethora of protein secretion types, rectifying misannotations and identifying some unrecognized major differences [42].

Among Gram-positive bacteria, two major subtypes are recognized: subtype A (T7SSa) and B (T7SSb). The T7SS was first discovered in *Mycobacterium tuberculosis* [15], and recent studies on Gram-positive bacteria have shown limited homology to the mycobacterial T7SS components, which led to the sub-classification into T7SSa (Actinobacteria) and T7SSb (Firmicutes) [16,17]. Both subtypes, however, are characterized by possessing a specialized transmembrane nanomachinery belonging to the FtsK/SpoIIIE ATPase protein family termed EccC (T7SSa) or EssC (T7SSb). Among the Actinobacteria, up to five paralogous subtypes are designated ESX systems (ESX-1–ESX-5) based on the T7SSa core components present [43]. In contrast, the Firmicutes have one prototype composed of four integral membrane components that form the complete core machinery, namely, EsaA, EssA, EsaB and EssB, all clustered on one operon [17,44].

Despite a limited structural similarity, T7SSs share highly similar substrates, including the early secretory antigenic targets (ESAT) A (EsxA) and B (EsxB), containing a conserved Trp–Xaa–Gly (WXG) central sequence motif. EsxA and EsxB are small acidic helical hairpins of ~100 amino acids that are secreted as folded dimers by the T7SS. The motif is crucial for proper folding, dimerization and, ultimately, targeting and translocation of the effector proteins through the T7SS [45]. The conserved WXG motif is centrally located at the hairpin hinge, giving the family its name, the WXG100 protein family [45,46]. Further, T7SS genes encoding additional WXG100-like proteins, EsxC and EsxD, have been identified in *Staphylococcus aureus*, and the polymorphic LXG toxin among Firmicutes and their functions have been characterized [24–26]. The TIGR04197 proteins have recently been linked to the T7SS based on phylogenetic profiling as a putative T7SS substrate. In addition, a site-specific mutation in the TIGR04197 encoding gene abrogated LXG effector export, suggesting its significance in

LXG effector secretion by the T7SSb apparatus in *Streptococcus intermedius* [47]. Secretion of these effectors, WXG100, WXG100-like and LXG toxins, depends on a functional EssC/EccC [17,26,48].

Many studies have been conducted on the T7SS in various species of public importance, however, none has focused on the secretion system in *B. cereus.* Its repertoire has not been reported but is always inferred from other Firmicutes members. Studies on the virulence of *B. cereus* have been biased towards enterotoxins associated with food poisoning symptoms. However, recent strains are increasingly causing more severe extra-intestinal and nosocomial infections [7,49]. Hence, there is a need to investigate other possible virulence mechanisms, such as the secretion system. Among the closely related *Bacillus* species, the T7SS has been characterised in *B. anthracis* [35] and *B. subtilis* [50,51].

Therefore, this study sought to identify the T7SSb gene locus and characterise the T7SSb-dependent effectors in *B. cereus.* By utilizing the genome of the type strain, *B. cereus* ATCC14579, the EssC encoding gene was identified by mapping to the well-studied T7SSb in *S. aureus* USA300. Further gene neighbourhood homology analysis established the genetic organization of T7SSb with notable variations downstream of the gene cluster. Furthermore, the standard strain, *B. cereus* ATCC14579, was used to identify T7SSb-dependent effectors. A comprehensive proteomic analysis of the culture supernatant for *B. cereus* ATCC14579 and its isogenic *ΔessC* mutant was conducted and identified two nearly identical (94%) EsxA proteins, EsxA1 and EsxA2.

Materials and methods

Genome sequence alignment and identification of core T7SSb gene cluster

The standard strain, *B. cereus* ATCC14579 (type strain), originally isolated from the environment [52], was selected as the standard strain from which other *B. cereus* strains will be compared. Among the Firmicutes, *S. aureus* T7SSb is well-studied, thus, it was chosen as the reference genome for homology and neighbourhood analysis. The GenBank files for *B. cereus* ATCC14579 (GenBank: NC_004722.1) and *S. aureus* USA300 (GenBank: CP092052.1) were downloaded from NCBI (https://www.ncbi.nlm.nih.gov/datasets/genome/) already annotated by NCBI Prokaryotic Genome Annotation Pipeline (PGAP) found at (https://www.ncbi.nlm.nih.gov/genome/annotation_prok/). The *B. cereus* ATCC14579 chromosome was compared to the reference *S. aureus* USA300 using Mauve (Darling lab, Australia) [53]. This analysis identified the T7SSb core machinery encoding genes in *B. cereus* ATCC14579, and the output data was imported into genoPlotR [54] to construct the gene cluster and visualization. Additionally, a comparative analysis of genome sequences was performed to detect T7SSb genes in the reference strain, *B. cereus* BC33 (GenBank: CP072774.1), and the more virulent clinical strains, *B. cereus* 30040 (ST1420) (GenBank: AP022975.1) and *B. cereus* B4264 (GenBank: CP001176.1) and the closely related species, *B. subtilis* 168 (GenBank: AL009126.3) and *B. anthracis* Sterne 32F2 (GenBank: AE017225.1) with pXO1 (GenBank: CP009540.1). SnapGene 5.0.8 software (GSL Biotech LLC, USA) was used to conduct a global sequence alignment (Neddleman-Wunsch) and calculated homologous T7SSb genes sequence similarity among the selected strains with reference to *B. cereus* ATCC14579.

Bacterial strains and growth conditions

For routine culture, *B. cereus* strains were grown in Brain Heart Infusion (BHI) medium (Difco, USA) and *Escherichia coli* strains in Luria-Bertani (LB) medium (Difco, USA) at 37°C (shaking at 155 rpm for liquid cultures). Bacterial cultures for genetic manipulation were grown on media (BHI or LB) containing antibiotics at final concentrations of 250 μg/ml (*B. cereus*) or 100 μg/ml (*E. coli*) spectinomycin, 60 units/ml polymyxin, 50 μg/ml kanamycin, and 100 μg/ml ampicillin. Cultures for protein liquid chromatography-tandem mass spectrometry were done in minimal medium (M9), 2% glucose, 50 mM Na_2HPO_4, 25 mM KH_2PO_4, 10 mM NaCl, 20 mM NH_4Cl, 1 mM $MgSO_4 \cdot 7H_2O$, 0.1 mM $CaCl_2$, 10 mM glutamic acid, 1.4 mM threonine, 0.6 mM leucine, 2.5 mM valine, 1.4 mM histidine and 0.3 mM methionine at 37°C.

Plasmid construction *for essC* deletion

Two plasmids were used to construct the *essC*-knockout strain, pRP1028, an *E. coli*-*Bacillus* shuttle vector, and pRP1099 to facilitate homologous recombination. Briefly, pRP1028 is a temperature-sensitive replicon in *Bacillus* with an *I-Sce*I site, a sequence encoding the red fluorescent protein (RFP) and spectinomycin resistance gene. The facilitator plasmid pRP1099 contains the genes for the *I-Sce*I enzyme under the control of a hybrid amylase promoter, green fluorescent protein (GFP) and kanamycin resistance. The bacterial strains and plasmids used in this study are shown in Table 1. The *essC* upstream (US) (*essB*) and downstream (DS) (*BC_RS10425*) homologous arms of *B. cereus* ATCC14579 were inserted into plasmid pRP1028 (Fig. 1) between the *Ban*II-*Sac*I and *Bsa*I sites to construct the pYF07 via Gibson Assembly (New England Biolabs Inc, England) [55]. The US and DS fragments were generated via PCR using the forward and reverse primers listed in Table 2. The resulting recombinant plasmid was transformed into heat-shock competent *E. coli* 10β cells for plasmid amplification. Plasmid DNA was purified by a QIAprep Spin Miniprep Kit (Qiagen, Germany). Briefly, PCR was carried out to confirm the plasmid assembly using KOD One Master Mix (TOYOBO, Japan) and diagnostic forward and reverse primers, pRP1028dx_F and pRP1028dx_R, respectively, whose sequences are shown in Table 2. The confirmed plasmid (pYF07) was subjected to sequencing PCR using a BigDye Terminator v3.1 Cycle Sequencing Kit (Applied Biosystems, USA) and subsequently sequenced using a 3130 Genetic Analyzer (Applied Biosystems, USA). The sequences were processed and aligned to the *B. cereus* genome to confirm sequence correctness and orientation using SnapGene 5.0.8 software (GSL Biotech LLC, USA).

Table 1. Bacterial strains and plasmids used in this study.

Strain	Genotype or Description	Source
B. cereus		
ATCC14579	Wild type (WT)	[52]
	ΔessC (*essC* gene deleted mutant)	This study
E. coli		
SM10	*thi thr leu tonA lacY supE recA::RP4-2-Tc::Mu (Km)*	[56]
S17-1	*thi, pro, hsdR, RP4-2 Tc::Mu Km::Tn7 (Tp Sm)*	[56]
10β	*Δ(ara-leu) 7697 araD139 fhuA ΔlacX74 galK16 galE15*	New England
(C3019H)	*e14- ϕ80dlacZΔM15 recA1 relA1 endA1 nupG rpsL (StrR)*	BioLabs
	rph spoT1 Δ(mrr-hsdRMS-mcrBC)	
Plasmids		
pRP1028	*Bacillus* and *E. coli* shuttle vector with *turbo-rfp* gene and an *I-SceI* recognition site; Spe^R	[57]
pRP1099	Vector with *turbo-AmCyan* and *I-SceI* genes; Kan^R	[57]
pYF07	pRP1028 with upstream and downstream regions of *essC*	This study

Spe^R and Kan^R, stand for spectinomycin and kanamycin resistance, respectively.

Table 2. Primers used for deletion of *essC* gene in *B. cereus* ATCC14579

Primer name	Sequence (5'–3')	Application
*essC*_US_F	cttgagctcctagcggccgcaagaaatgagaaattaagactacttcgg	US fragment
*essC*_US_R	ttaatttcagaattccatccgtgttcactgctc	amplification
*essC*_DS_F	acacggatggaattctgaaattaaagaagaaagctaaggtg	DS fragment
*essC*_DS_R	gtacaggtctccggccgctctgcgttaaatttatcctgtaatgtc	amplification
pRP1028dx_F	ggctgacgccgttggatacacc	Confirmation of
pRP1028dx_R	gcccgtcacgggcttctcagggc	pYF07 assembly
*essC*_F	gctgtattggatgtataacgg	Diagnosis for *essC*
*essC*_R	cgcttgtgttgtacttcc	deletion

Markerless deletion of *essC* in *B. cereus* ATCC14579

The allelic exchange system used in this study was developed based on the homing endonuclease *I-Sce*I mediated markerless gene replacement method established in *B. anthracis* [57] with minor variations. We used the biparental mating method, eliminating the use of the helper strain (*E. coli* SS1827). We used *E. coli* SM10 and S17-1, which have *tra* genes encoding factors that can mobilize *oriT*-containing plasmids and integrate into chromosomes, thus making biparental mating possible. *E. coli* SM10 cells were transformed with the recombinant shuttle vector pYF07. The transformed *E. coli* SM10 cells (donor strain) were grown on LB agar with 100 µg/ml spectinomycin at 37°C overnight. *B. cereus* ATCC14579 (recipient strain) was also grown on BHI at 37°C overnight. Colony blobs of the donor and recipient strains were placed on BHI agar, mixed evenly, then spread on the entire plate, and incubated at room temperature for 24 h. The growth was swabbed onto BHI containing 250 µg/ml spectinomycin and 60 units/ml polymyxin B (BHI-Spe-Pmx) and incubated at room temperature for 48 h for conjugant *B. cereus* colony isolation. After twice passaging on BHI-Spe-Pmx incubated at 37°C overnight, pink-coloured *B. cereus* colonies were checked for red fluorescence using LAS 400 Luminescent Image Analyzer (GE Healthcare, USA) with RFP Green (Epi-RGB) setting. Colonies that gave a positive fluorescent signal were swabbed together with *E. coli* S17-1 harbouring pRP1099 in BHI containing 50 µg/ml kanamycin and 60 units/ml polymyxin B and incubated at 37°C overnight. Spectinomycin-sensitive and RFP-negative *B. cereus* colonies were plated on BHI and incubated at 37°C overnight twice to lose the pRP1099 plasmid. Finally, the kanamycin-sensitive and GFP-negative colonies were confirmed to possess the desired deletion using PCR (primers *essC*_F and *essC*_R are shown in Table 2) and sanger sequencing. This allelic exchange procedure is illustrated in Figure 1.

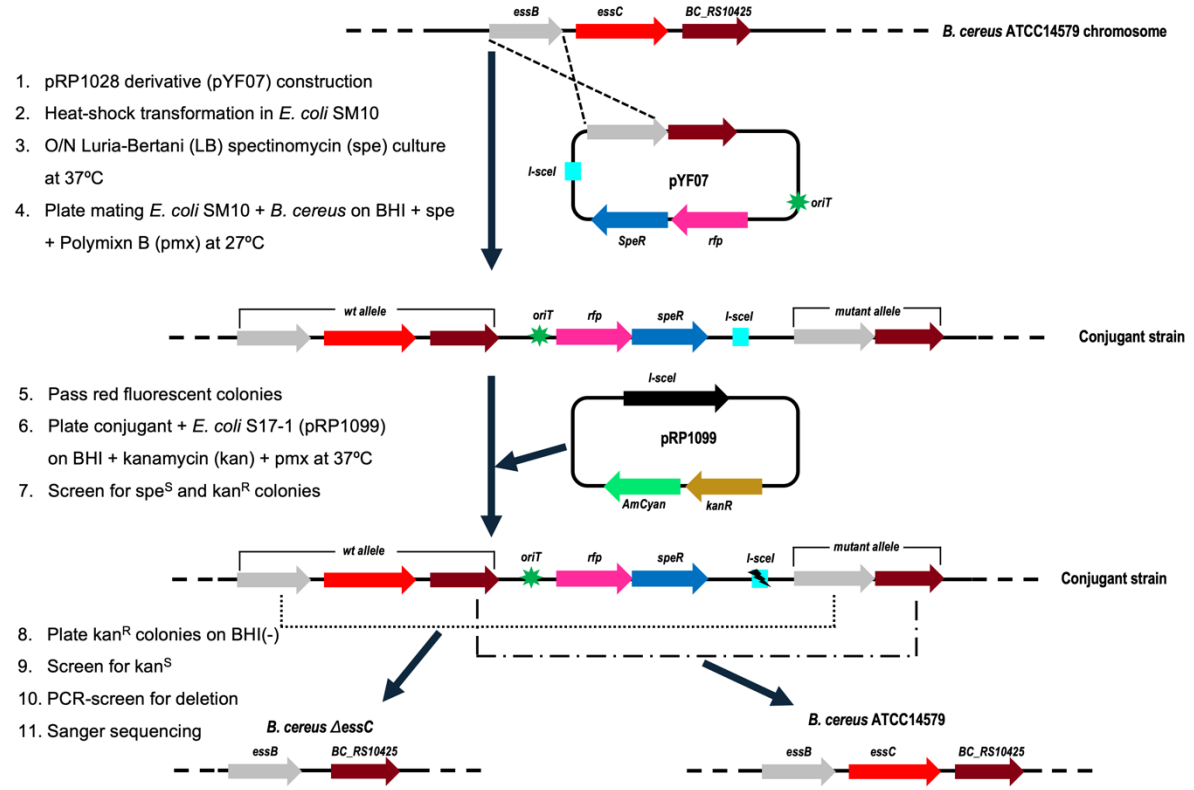

Figure 1. Schematic summary of the allelic exchange system used for generating desired gene deletions.

Liquid chromatography-tandem mass spectrometry to identify the effector proteins of *B. cereus* T7SSb

B. cereus ATCC14579 and its *ΔessC* mutant were each grown in 2.5 ml LB at 37°C for 18 h, and then cells were pelleted and washed three times in M9. Resuspended cells were incubated in M9 with start OD_{600} = 0.05 at 37°C until mid-log phase (~5 h). The cells were pelleted and filtered the culture supernatant using a 0.45 μm membrane filter (Millipore, Ireland). The supernatant was purified using methanol-based C8 reverse-phase liquid chromatography (Strata™ Phenomenex, USA). The purified protein mixture then underwent alkylation, tryptic digestion, and further peptide purification using Pierce™ C18 spin columns (ThermoFisher Scientific, USA) following the manufacturer's protocol. The peptide mixtures were analyzed using the HPLC liquid phase system EASY nLC1000 (ThermoFisher Scientific, USA). They were loaded onto a C18 column (3 μm particle diameter, 0.075 mm x 120 mm, Nikkyo Technos, Japan) at a 300 nl/min flow rate controlled by intelliflow technology over 81 min. The HPLC was coupled online via a nanoelectrospray ion source to a hybrid ion trap quadrupole-Orbitrap (LTQ–OrbitrapXL; ThermoFisher Scientific) tandem mass spectrometer (LC-MS/MS) [58]. The LC−MS/MS.RAW files were searched against *B. cereus* ATCC 14579 protein FASTA file database and annotated the peptides using the Sequest HT algorithm in Proteome Discoverer 1.4.1.14 (DBVersion:79) (Thermo Fisher Scientific, USA). The reference strain *B. cereus* BC33 (GenBank: CP072774.1) was also used as a database to validate the peptide annotations from the *B. cereus* ATCC14579 database. Search parameters were set to two missed trypsin cleavage sites, and a precursor mass tolerance of 10 ppm and a fragment mass tolerance of 0.06 Da were utilized. The search included carbamidomethylation of cysteine as a static modification and amine carbamylation and methionine oxidation as dynamic modifications, with a maximum of four modifications per peptide. The false discovery rate for peptide-spectrum matches (PSMs) was set at 1% maximum using a target-decoy PSM validator [59,60].

Sequences of annotated proteins in the mass spectrometry data were obtained from the GenBank files and analyzed for motifs found among known T7SS substrates using the GenomeNet platform [61] to validate their identity. Further bioinformatic searches were conducted using web resources NCBI BLASTp [62] (available at https://blast.ncbi.nlm.nih.gov/Blast.cgi) to obtain the best hits among Firmicutes for CLUSTAL O alignment. Furthermore, using the established effector protein sequences, their encoding genes were identified using NCBI TBLASTn. The effector protein genes were then compared to other *Bacillus* species to complete the genetic organization of the T7SSb.

Protein structure modeling

The protein sequences of EsxA1 and EsxA2 were obtained from the *B. cereus* ATCC14579 GenBank file (GenBank: NC_004722.1). The sequences in FASTA format were uploaded into Swiss-Model Workspace via Expasy web server program [63]. The models were built with default settings. The pdb output files were imported into MacPyMOL software version 3.0 [64] for further manipulations, analyses and construction of molecular model structures.

Results

Organization and characteristics of T7SSb gene cluster in *B. cereus*

In-silico gene neighbourhood analysis and results from mass spectrometry established the T7SSb locus in *B. cereus* ATCC14579 (Fig. 2). With *S. aureus* USA300 [24,48] as the reference genome, the five T7SSb core genes in *B. cereus* ATCC14579 were identified, all arranged similar to *S. aureus* USA300 on the same operon. Overall sequence homology was low, averaging below 52%, with the lowest being *esaA* and *essA* at 48% and *essC* the highest at 56%. When compared among *B. cereus* strains, core genes' sequence homology was nearly identical, with most genes being more than 93% similar. In contrast, the *B. subtilis* 168 core T7SSb genes possess very low homology, all below 47%. Although the genes are tandem, the arrangement differs from *B. cereus* and *S. aureus*. On the other hand, *B. anthracis* Sterne 32F2 possess an unusual T7SS with *esaB* and *essC* as the only core components of the T7SSb machinery.

Further analysis of *B. cereus* strains showed that the T7SSb gene cluster is conserved up to 5' two-thirds of the *essC* encoding the ATPase domain indispensable for secretion of T7SSb-dependent effectors. One-third on the 3' end of *essC* and the ensuing genes within the T7SSb cluster showed variation among the standard strains, *B. cereus* ATCC14579 and *B. cereus* BC33 (Fig. 2; Fig. 3). The variable region in the clinical isolates, *B. cereus* 30040 and *B. cereus* B4264, possesses a second TIGR04197 protein and LXG toxin genes within the cluster. In contrast, the variable region in *S. aureus* encodes other T7SSb effectors, EsxB, EsxC, EsxD, and LXG toxin, including immunity proteins (Fig. 2). LXG toxins are diverse and polymorphic, with N-terminal LXG delivery domains and diverse C-terminal toxin domains that mediate intercellular competition in biofilms via the T7SS in *S. aureus* and *B. subtilis* [65,66].

Similarly, the *B. anthracis* variable region has a single copy of the EsxB encoding gene with additional genes that are part of the toxin-antitoxin (TA) cluster. Interestingly, within the TA cluster, there is an *sseB* gene that encodes an EspA protein that forms part of the T3SS translocon [67,68]. Furthermore, the *B. anthracis* genome does not possess esxA but has multiple genes encoding WXG100-like proteins. Next to *sseB* is *esxL*, which encodes WXG100-like proteins like those found in *S. aureus*. BLAST search analysis found that *B. anthracis* possesses additional WXG100-like proteins, EsxP, EsxQ, EsxV and EsxW, that are encoded elsewhere on the plasmid pXO1 and distant sites on the chromosome that are far from *essC* as shown in Figure 4A. It was also noted that *esxL, esxQ, and esxP* are immediately upstream of an immunity protein on the same operon that forms part of the TA system (Fig.

4A). This finding gives a clue about the link between the *B. anthracis* secretion systems and its TA system, a relationship that has been established in *Pseudomonas aeruginosa* [69,70]. CLUSTAL O multiple sequence alignment and phylogenetic analysis of the WXG100-like proteins showed that EsxL is more closely related to EsxC of *S. aureus* than those native to *B. anthracis* (Fig. 4B).

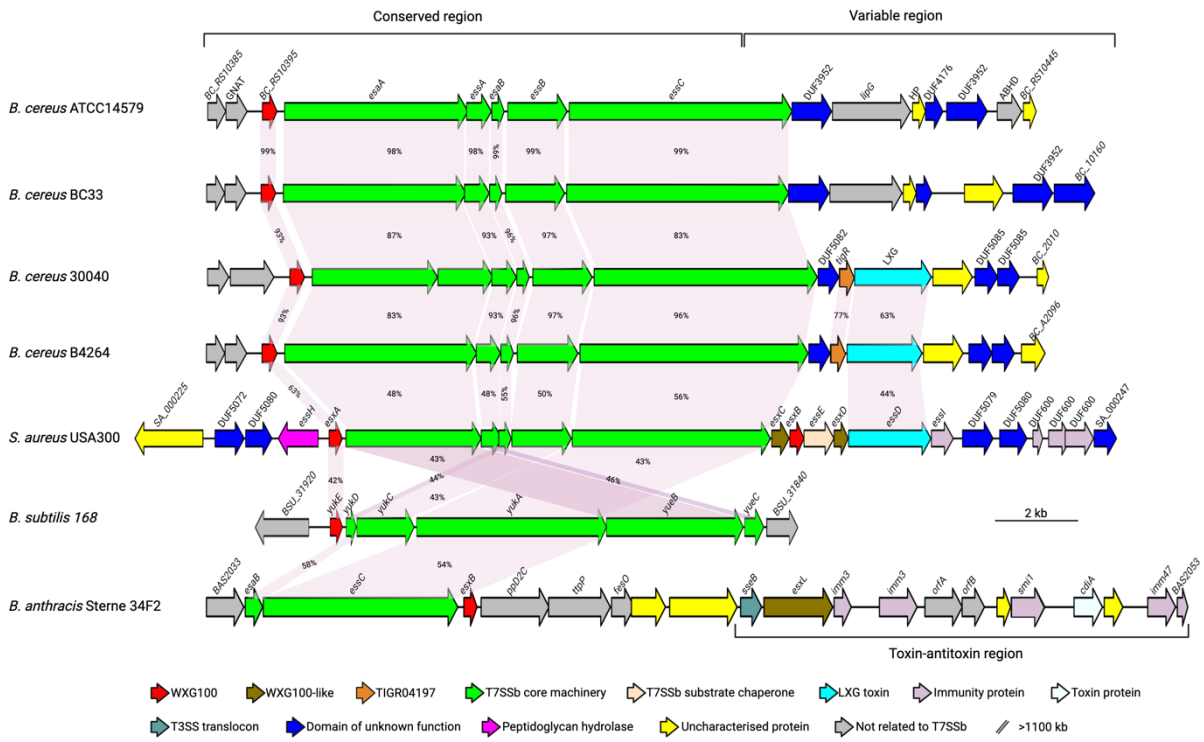

Figure 2. Schematic representation of the T7SSb gene cluster in *Bacillus* species.

Homology of the corresponding T7SSb gene clusters in different *B. cereus* strains *S. aureus* USA300, *B. subtilis* 168 and *B. anthracis* 34F2 are also shown. The same colour indicates related genes, and percentage identities for each gene, with reference to *B. cereus* ATCC14579, are shown in pink-shaded areas. For the LXG gene, the reference strain is *B. cereus* 30040. All *Bacillus* species possessed one WXG100 protein-encoding gene, being the first gene in the T7SS cluster in *B. cereus* and *B. subtilis,* while in *B. anthracis,* it is downstream of the core machinery genes. Genes at the 5' end of the *essC* are highly conserved, while variation is observed in the 3' end. Notice that *B. anthracis* 34F2 possess two core genes, *esaB* and *essC*, a single copy of *esxB* and a TA gene cluster downstream of T7SS machinery. In addition, B. anthracis possesses *sseB*, which encodes a T3SS translocon essential for virulence and pathogenicity in *Salmonella* species.

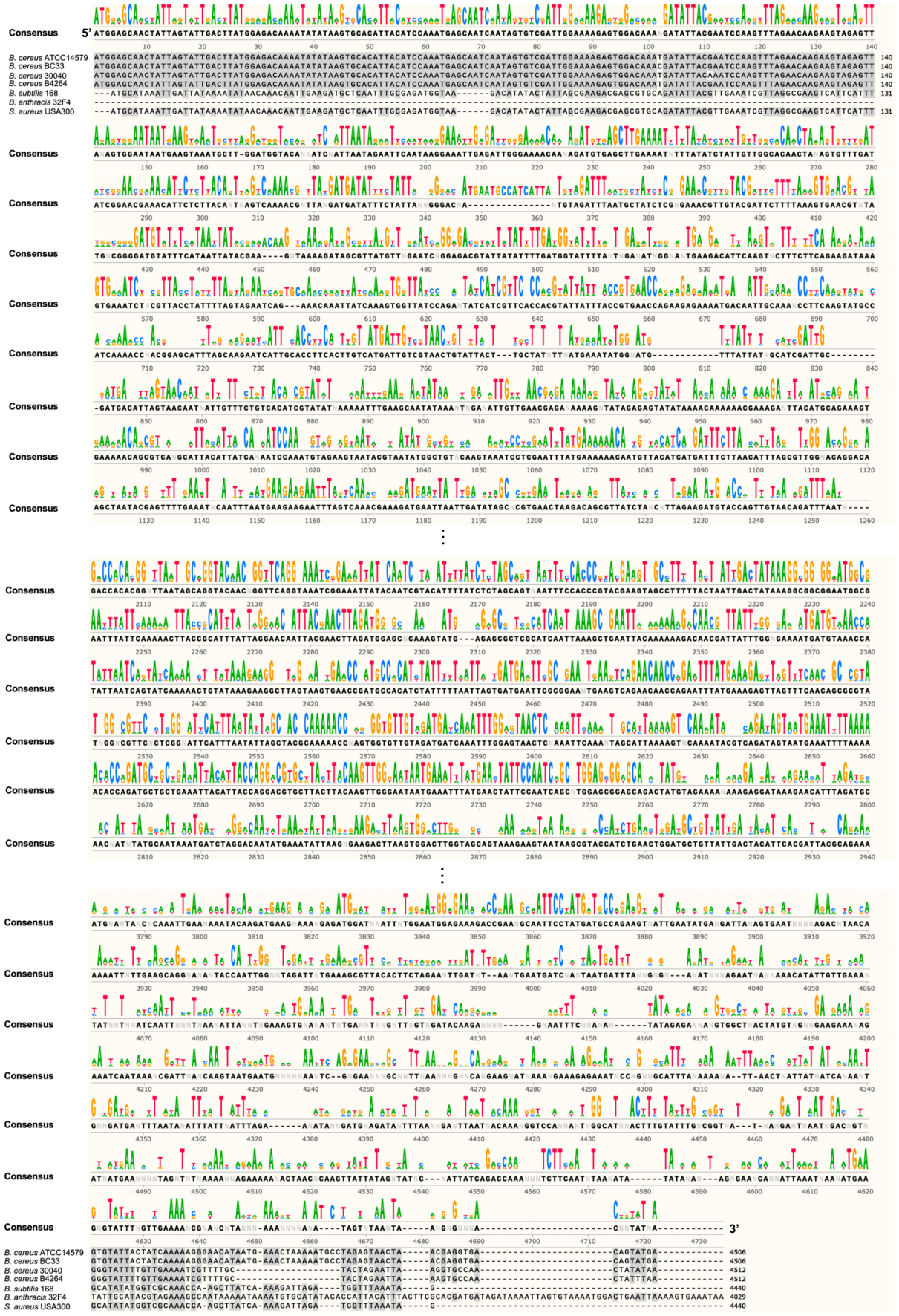

Figure 3. The proximal, middle and distal sequence alignments of *essC* in *Bacillus* species

and *S. aureus*.

Positions with a mix of nucleotides (represented by N) and gaps (represented by -) appear with the highest frequency at the 3’ end compared to the 5’ end in the consensus sequence. The locations with a mix of nucleotides indicate species and strain-specific variation and the gaps indicate insertions or deletions in one or more sequences relative to others. Thus, the 3’ end possesses more diversity than the 5’ end. The consensus sequence was set at a minimum threshold of 50%.

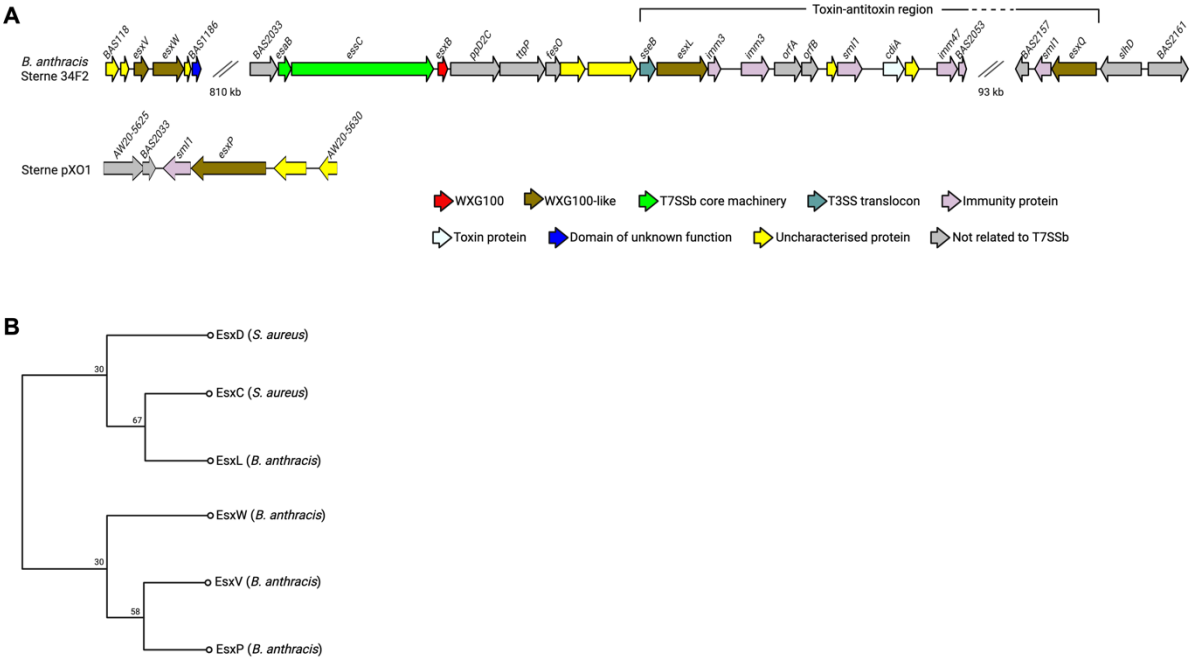

Figure 4. *B. anthracis* T7SSb effector genes are scattered across the genome and pXO1.

A. The *B. anthracis* T7SSb is located on four islands, three of which are in the genome and one on the plasmid pXO1. Note that *esxL*, *esxQ,* and *esxP* are immediately upstream of an immunity protein on the same operon that forms part of the TA system.

B. Phylogenetic relationships of the WXG100-like proteins in *B. anthracis* and *S. aureus*. The values at each node represent bootstrap percentage values for branch support. EsxL (*B. anthracis*) is closely related to EsxC of *S. aureus,* which has a high branch support of 67%.

Deletion of *essC* in *B. cereus* ATCC14579

Conjugation of *B. cereus* with pRP1028 derivatives carrying complete *essC* deletion (4,498 bp) was flanked by 1,002 bp (US) and 1,000 bp (DS) homologous sequences. After incubations were conducted at the non-permissive temperature for plasmid replication (37°C), growth was visualized grossly using ImageQuant LAS 4000 Luminescent Image Analyzer (GE Healthcare, USA) with RFP Green (Epi-RGB) setting. Colonies in which the shuttle plasmid was integrated into *B. cereus* genomic DNA following crossover by homologous recombination appeared as pink-reddish colonies grossly (Fig. 5A) and black under green-fluorescent light (Fig. 5B). In a second round of conjugation, pRP1099 that was transferred to the integrant, stimulated the second crossover by expression of I-SceI and cleavage of the integrated plasmid. Re-imaging for TurboRFP expression allowed visualization of non-fluorescent colonies (grey colour) that have lost the integrated pRP1028 derivative following a second crossover event (Fig. 5C). PCR screening of non-fluorescent colonies confirmed the deletion of *essC* in the *B. cereus* genome (Fig. 5D).

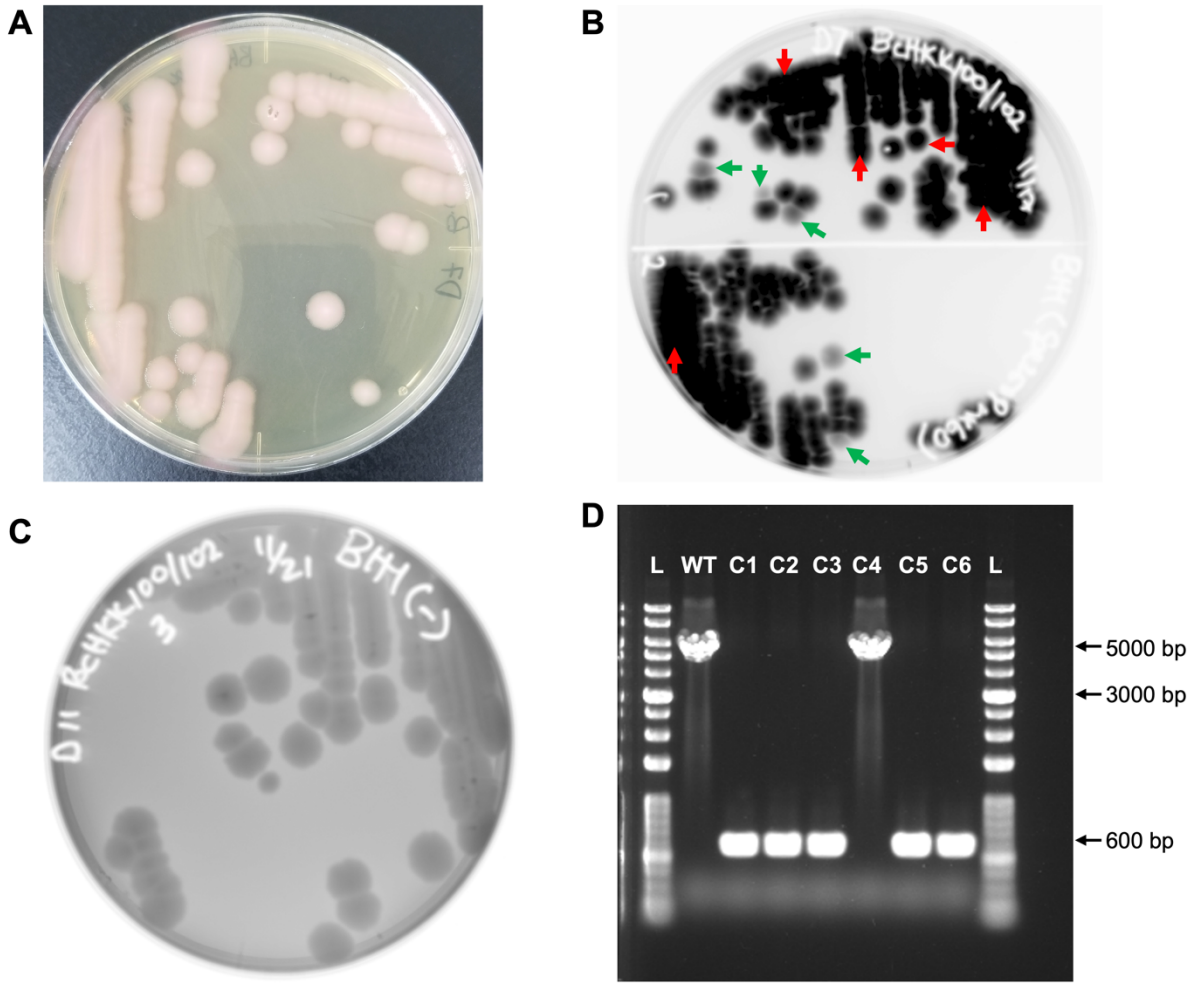

Figure 5. pRP1028 derivative chromosomal integration and *essC* deletion in *B. cereus* ATCC14579.

A. Pink-coloured colonies for *B. cereus* indicating successful chromosomal integration of pRP1028 derivative (pYF07) after incubation at 37°C overnight.

B. Visualization of *B. cereus* colonies under RFP Green (Epi-RGB) light showing positive (red arrows) and negative (green arrows) fluorescent signals.

C. Non-fluorescent colonies under RFP Green (Epi-RGB) light after the second crossover indicate loss of previously integrated pRP1028.

D. Colony PCR using primers *essC*_F and *essC*_R to confirm *essC* deletion with the wild type (WT) as positive control (5,097 bp). Sample colonies C1–C3, C5 and C6 with almost 600 bp products indicate deletion of *essC* (4,498 bp). Colony C4 yielded a product similar to the WT, which meant that the pYF07 conjugant reverted to the wild-type allele. L = DNA ladder.

B. cereus possesses two ESAT-6-like T7SSb-dependent effectors

To identify the *B. cereus* T7SSb-dependent effector proteins, first, we generated the *ΔessC* mutant using *B. cereus* ATCC14579. The mid-log phase M9 culture of *B. cereus* ATCC14579 (WT) and its *ΔessC* mutant were utilized in the secretome analyses to identify the T7SSb-dependent effectors. From the LC-MS/MS raw data, the search algorithm in Proteome Discoverer identified 92 proteins in the WT and 77 proteins in the *ΔessC* mutant for three independent experiments (Tables 3 and 4). To increase confidence in the identifications, we limited our analysis to those proteins identified by two or more peptides. Analysis for protein identification overlap showed 62% (57/92) and 74% (57/77) protein identification for all three biological experiments together in the WT and *ΔessC*, respectively. Of the 92 proteins in the secretome of WT, only two were annotated as ESAT-6-like [*Bacillus cereus*]. No ESAT-6-like protein was found in the secretome for the *ΔessC* strain (Fig. 6). The protein annotations (NCBI RefSeq) and their descriptions for the WT are shown in Table 3, and for the *ΔessC* strain in Table 4. Motif search analysis of the secretomes in GenomeNet (Kyoto University Bioinformatics Center) confirmed that the two proteins designated Q81HA0 and Q81EA6 were categorized as T7SS effectors. Proteins that did not possess known motifs related to the T7SS were excluded from further analyses.

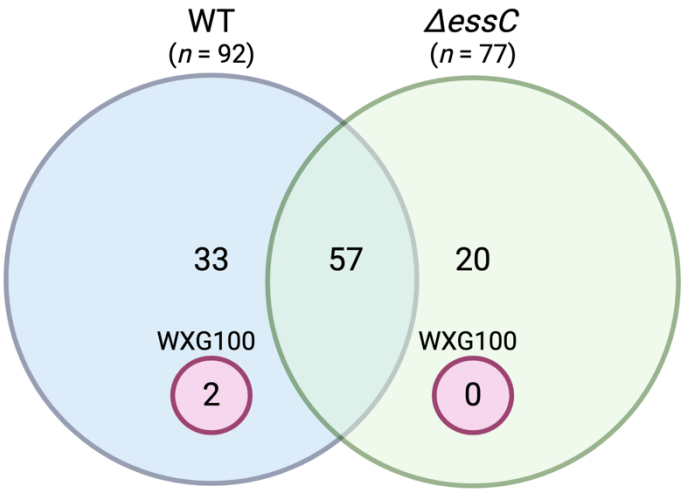

Figure 6. Venn plot illustrating mass spectrometry protein identification in the wild type and *ΔessC*.

The wild-type secretome had 62% (57/92) protein overlap, while *ΔessC* had 74% (57/77) across the three biological experiments. Only two proteins were identified to belong to the WXG100 superfamily in the WT and none in *ΔessC*.

Table 3. Proteins identified in the secretome of *B. cereus* ATCC14579. Accession numbers (NCBI RefSeq) in bold indicate proteins unique to the wild type. The WXG100 proteins are written in red. These results represent data obtained from three independent experiments.

		Wild type
#	**Accession**	**Description**
1	P62171	Cold shock-like protein CspC OS=*Bacillus cereus*
2	**P62175**	30S ribosomal protein S13 OS=*Bacillus cereus*
3	Q812X3	Elongation factor Ts OS=*Bacillus cereus*
4	Q812X4	Ribosome-recycling factor OS=*Bacillus cereus*
5	**Q813P2**	Non-specific DNA-binding protein Dps/ Ferroxidase OS=*Bacillus cereus*
6	**Q813Q6**	Non-expressed Enterotoxin C OS=*Bacillus cereus*
7	**Q813W0**	Endonuclease/Exonuclease/phosphatase family protein OS=*Bacillus cereus*
8	Q814B1	Co-chaperonin GroES OS=*Bacillus cereus*
9	Q814C4	Elongation factor Tu OS=*Bacillus cereus*
10	Q814C5	Elongation factor G OS=*Bacillus cereus*
11	Q814S1	Bacillolysin OS=*Bacillus cereus*
12	Q814S3	PapR protein OS=*Bacillus cereus*
13	Q815D2	Phosphoglycerol transferase OS=*Bacillus cereus*
14	Q815G3	N-acetylmuramoyl-L-alanine amidase OS=*Bacillus cereus*
15	**Q815H1**	Tail-specific protease OS=*Bacillus cereus*
16	Q815K6	Glyceraldehyde-3-phosphate dehydrogenase OS=*Bacillus cereus*
17	**Q815X1**	3-ketoacyl-CoA thiolase OS=*Bacillus cereus*
18	Q815X2	Acyl-CoA dehydrogenase OS=*Bacillus cereus*
19	Q815Y3	Glycine cleavage system H protein OS=*Bacillus cereus*
20	Q816H3	Cold shock-like protein CspD OS=*Bacillus cereus*
21	Q816H9	1,4-dihydroxy-2-naphthoyl-CoA synthase OS=*Bacillus cereus*
22	Q816M6	Phage shock protein A OS=*Bacillus cereus*
23	Q817A0	Acetyl-coenzyme A synthetase OS=*Bacillus cereus*
24	Q817D1	Universal stress protein OS=*Bacillus cereus*
25	Q817D3	Alanine dehydrogenase OS=*Bacillus cereus*
26	Q817L7	Electron transfer flavoprotein beta-subunit OS=*Bacillus cereus*
27	Q817L8	Thioredoxin OS=*Bacillus cereus*
28	Q817U2	50S ribosomal protein L21 OS=*Bacillus cereus*
29	Q817U4	50S ribosomal protein L27 OS=*Bacillus cereus*
30	Q817Z6	Transcription elongation factor GreA OS=*Bacillus cereus*
31	**Q818A5**	Ferrichrome-binding protein OS=*Bacillus cereus*
32	Q818E9	Chaperone protein DnaK OS=*Bacillus cereus*
33	Q818M3	Aminomethyltransferase OS=*Bacillus cereus*
34	Q818U1	Arginine-binding protein OS=*Bacillus cereus*
35	Q818U8	Peptidase T OS=*Bacillus cereus*
36	Q819H7	5-methyltetrahydropteroyltriglutamate-homocysteine methyltransferase OS=*B. cereus*
37	Q819M9	Pyruvate carboxylase OS=*Bacillus cereus*
37	Q819Q2	UDP-N-acetylmuramoylalanine--D-glutamate ligase OS=*Bacillus cereus*
39	Q819S3	Carbamoyl-phosphate synthase large chain OS=*Bacillus cereus*
40	Q819V7	Acyl carrier protein OS=*Bacillus cereus*
41	Q819X0	Succinate--CoA ligase [ADP-forming] subunit beta OS=*Bacillus cereus*
42	Q819X8	GTP-sensing transcriptional pleiotropic repressor CodY OS=*Bacillus cereus*
43	Q81A05	Nucleoside-binding protein OS=*Bacillus cereus*
44	Q81AF6	Aconitate hydratase OS=*Bacillus cereus*
45	Q81AG8	Protease HhoA OS=*Bacillus cereus*

		Wild type
#	Accession	Description
47	Q81AK8	Aldehyde dehydrogenase OS=*Bacillus cereus*
48	Q81AM3	Cold shock protein OS=*Bacillus cereus*
49	Q81B13	Neutral metalloproteinase OS=*Bacillus cereus*
50	**Q81BE4**	Surface protein OS=*Bacillus cereus*
51	**Q81BM1**	General stress protein 17M OS=*Bacillus cereus*
52	Q81BP9	Hemolysin BL binding component OS=*Bacillus cereus*
53	**Q81BS6**	Signal peptidase I OS=*Bacillus cereus*
54	**Q81C25**	Probable malate:quinone oxidoreductase OS=*Bacillus cereus*
55	Q81C48	ABC transporter ATP-binding protein OS=*Bacillus cereus*
56	Q81CL9	Neutral metalloproteinase OS=*Bacillus cereus*
57	Q81D73	Bacillolysin OS=*Bacillus cereus*
58	Q81D88	Propionyl-CoA carboxylase beta chain OS=*Bacillus cereus*
59	Q81DP3	DNA-binding protein HU OS=*Bacillus cereus*
60	Q81DR7	Acyl-CoA dehydrogenase OS=*Bacillus cereus*
61	Q81DR8	Methylisocitrate lyase OS=*Bacillus cereus*
62	Q81DX6	Alcohol dehydrogenase OS=*Bacillus cereus*
63	**Q81DY5**	Uncharacterized protein OS=*Bacillus cereus*
64	Q81E03	Serine-type D-Ala-D-Ala carboxypeptidase OS=*Bacillus cereus*
65	**Q81EA6**	ESAT-6-like protein OS=*Bacillus cereus*
66	Q81EI5	Putative murein endopeptidase OS=*Bacillus cereus*
67	Q81EZ8	Non-hemolytic enterotoxin lytic component L2 OS=*Bacillus cereus*
68	Q81FD4	Flagellin OS=*Bacillus cereus*
69	Q81FD5	Flagellin OS=*Bacillus cereus*
70	Q81FI2	Cold shock protein OS=*Bacillus cereus*
71	**Q81FQ9**	DNA-binding protein HU OS=*Bacillus cereus*
72	**Q81FS1**	SSU ribosomal protein S1P OS=*Bacillus cereus*
73	**Q81FT6**	Ferredoxin OS=*Bacillus cereus*
74	**Q81GC3**	Immune inhibitor A OS=*Bacillus cereus*
75	**Q81H27**	General stress protein 17M OS=*Bacillus cereus*
76	**Q81HA0**	ESAT-6-like protein OS=*Bacillus cereus*
77	**Q81HD5**	UPF0342 protein BC_0880 OS=*Bacillus cereus*
78	**Q81HJ4**	Enterotoxin/cell-wall binding protein OS=*Bacillus cereus*
79	**Q81HU4**	IG hypothetical 22578 OS=*Bacillus cereus*
80	**Q81HW5**	Immune inhibitor A OS=*Bacillus cereus*
81	**Q81I30**	Alanine dehydrogenase OS=*Bacillus cereus*
82	**Q81IA3**	Formate acetyltransferase OS=*Bacillus cereus*
83	**Q81IP0**	1-pyrroline-5-carboxylate dehydrogenase OS=*Bacillus cereus*
84	**Q81J01**	Glutamine--fructose-6-phosphate aminotransferase [isomerizing] OS=*Bacillus cereus*
85	**Q81J17**	50S ribosomal protein L17 OS=*Bacillus cereus*
86	**Q81J23**	50S ribosomal protein L15 OS=*Bacillus cereus*
87	**Q81J25**	30S ribosomal protein S5 OS=*Bacillus cereus*
88	**Q81J30**	50S ribosomal protein L5 OS=*Bacillus cereus*
89	**Q81J43**	30S ribosomal protein S10 OS=*Bacillus cereus*
90	**Q81J48**	DNA-directed RNA polymerase subunit beta OS=*Bacillus cereus*
91	**Q81J50**	50S ribosomal protein L7/L12 OS=*Bacillus cereus*
92	**Q81J66**	Negative regulator of genetic competence clpC/mecB OS=*Bacillus cereus*

Table 4. Proteins identified in the secretome of *B. cereus* ATCC14579 *ΔessC*. Accession numbers (NCBI RefSeq) in bold indicate proteins unique to the *ΔessC* strain. These results represent data obtained from three independent experiments.

		ΔessC
#	**Accession**	**Description**
1	P62171	Cold shock-like protein CspC OS=*Bacillus cereus*
2	**Q7BYC6**	Hemolysin BL lytic component L1 OS=*Bacillus cereus*
3	Q812X3	Elongation factor Ts OS=*Bacillus cereus*
4	Q812X4	Ribosome-recycling factor OS=*Bacillus cereus*
5	Q814B1	Co-chaperonin GroES OS=*Bacillus cereus*
6	Q814C4	Elongation factor Tu OS=*Bacillus cereus*
7	Q814C5	Elongation factor G OS=*Bacillus cereus*
8	**Q814R4**	Collagen adhesion protein OS=*Bacillus cereus*
9	Q814S1	Bacillolysin OS=*Bacillus cereus*
10	Q815D2	Phosphoglycerol transferase OS=*Bacillus cereus*
11	Q815G3	N-acetylmuramoyl-L-alanine amidase OS=*Bacillus cereus*
12	Q815K6	Glyceraldehyde-3-phosphate dehydrogenase OS=*Bacillus cereus*
13	Q815X2	Acyl-CoA dehydrogenase OS=*Bacillus cereus*
14	Q815Y3	Glycine cleavage system H protein OS=*Bacillus cereus*
15	Q816H3	Cold shock-like protein CspD OS=*Bacillus cereus*
16	Q816H9	1,4-dihydroxy-2-naphthoyl-CoA synthase OS=*Bacillus cereus*
17	Q816M6	Phage shock protein A OS=*Bacillus cereus*
18	**Q816X7**	Ribosomal-protein-serine acetyltransferase OS=*Bacillus cereus*
19	Q817A0	Acetyl-coenzyme A synthetase OS=*Bacillus cereus*
20	Q817D1	Universal stress protein OS=*Bacillus cereus*
21	Q817D3	Alanine dehydrogenase OS=*Bacillus cereus*
22	**Q817J5**	Cell surface protein OS=*Bacillus cereus*
23	**Q817J7**	Cell surface protein OS=*Bacillus cereus*
24	Q817L7	Electron transfer flavoprotein beta-subunit OS=*Bacillus cereus*
25	Q817L8	Thioredoxin OS=*Bacillus cereus*
26	**Q817R8**	Stage II sporulation protein B OS=*Bacillus cereus*
27	Q817U2	50S ribosomal protein L21 OS=*Bacillus cereus*
28	Q817U4	50S ribosomal protein L27 OS=*Bacillus cereus*
29	Q817Z6	Transcription elongation factor GreA OS=*Bacillus cereus*
30	Q818E9	Chaperone protein DnaK OS=*Bacillus cereus*
31	**Q818G9**	Membrane-attached cytochrome c550 OS=*Bacillus cereus*
32	Q818M3	Aminomethyltransferase OS=*Bacillus cereus*
33	Q818U1	Arginine-binding protein OS=*Bacillus cereus*
34	Q818U8	Peptidase T OS=*Bacillus cereus*
35	Q819H7	5-methyltetrahydropteroyltriglutamate-homocysteine methyltransferase OS=*B. cereus*
36	Q819M9	Pyruvate carboxylase OS=*Bacillus cereus*
37	Q819P9	Cell division protein FtsL OS=*Bacillus cereus*
37	Q819Q2	UDP-N-acetylmuramoylalanine--D-glutamate ligase OS=*Bacillus cereus*
39	**Q819Q7**	Cell division protein FtsZ OS=*Bacillus cereus*
40	Q819S3	Carbamoyl-phosphate synthase large chain OS=*Bacillus cereus*
41	Q819V7	Acyl carrier protein OS=*Bacillus cereus*
42	Q819X0	Succinate--CoA ligase [ADP-forming] subunit beta OS=*Bacillus cereus*
43	Q819X8	GTP-sensing transcriptional pleiotropic repressor CodY OS=*Bacillus cereus*
44	Q81A05	Nucleoside-binding protein OS=*Bacillus cereus*
45	**Q81A31**	Microbial collagenase OS=*Bacillus cereus*

		ΔessC
#	**Accession**	**Description**
46	Q81AF6	Aconitate hydratase OS=*Bacillus cereus*
47	Q81AG8	Protease HhoA OS=*Bacillus cereus*
48	Q81AI2	Oligopeptide-binding protein oppA OS=*Bacillus cereus*
49	Q81AK8	Aldehyde dehydrogenase OS=*Bacillus cereus*
50	Q81AM3	Cold shock protein OS=*Bacillus cereus*
51	**Q81AM9**	Vancomycin B-type resistance protein vanW OS=*Bacillus cereus*
52	**Q81AN8**	Hemolysin II OS=*Bacillus cereus*
53	**Q81AY5**	Microbial collagenase OS=*Bacillus cereus*
54	Q81B13	Neutral metalloproteinase OS=*Bacillus cereus*
55	**Q81BN1**	5'-nucleotidase OS=*Bacillus cereus*
56	Q81BP9	Hemolysin BL binding component OS=*Bacillus cereus*
57	**Q81C01**	Immune inhibitor A OS=*Bacillus cereus*
58	Q81C25	Probable malate:quinone oxidoreductase OS=*Bacillus cereus*
59	Q81C48	ABC transporter ATP-binding protein OS=*Bacillus cereus*
60	Q81CL9	Neutral metalloproteinase OS=*Bacillus cereus*
61	Q81D73	Bacillolysin OS=*Bacillus cereus*
62	Q81D88	Propionyl-CoA carboxylase beta chain OS=*Bacillus cereus*
63	Q81DP3	DNA-binding protein HU OS=*Bacillus cereus*
64	Q81DR7	Acyl-CoA dehydrogenase OS=*Bacillus cereus*
65	Q81DR8	Methylisocitrate lyase OS=*Bacillus cereus*
66	Q81DX6	Alcohol dehydrogenase OS=*Bacillus cereus*
67	Q81E03	Serine-type D-Ala-D-Ala carboxypeptidase OS=*Bacillus cereus*
68	Q81EI5	Putative murein endopeptidase OS=*Bacillus cereus*
69	Q81EZ8	Non-hemolytic enterotoxin lytic component L2 OS=*Bacillus cereus*
70	Q81FD4	Flagellin OS=*Bacillus cereus*
71	Q81FD5	Flagellin OS=*Bacillus cereus*
72	Q81FI2	Cold shock protein OS=*Bacillus cereus*
73	**Q81FY1**	Cell wall endopeptidase, family M23/M37 OS=*Bacillus cereus*
74	**Q81GC6**	Cell envelope-bound metalloprotease (Camelysin) OS=*Bacillus cereus*
75	**Q81GS6**	Cytotoxin K OS=*Bacillus cereus*
76	**Q81HJ1**	Periplasmic component of efflux system OS=*Bacillus cereus*
77	**Q81HV2**	Cell wall-binding protein OS=*Bacillus cereus*

Characteristics of ESAT-6-like proteins found in the wild-type secretome

The amino acid sequences for the ESAT-6-like found in the secretome of the *B. cereus* ATCC14579 aligned locally (Smith-Waternan) using SnapGene 5.0.8 (GSL Biotech LLC, USA). They were found to have a sequence identity of 93.9% (92/98), and 96.9% (95/98) of the amino acids were similar. Amino acids at positions 17, 31 and 86 were different, while those on positions 18, 90 and 98 were similar (Fig. 7A). Figure 7B shows the 3-dimensional model structures of EsxA1 and EsxA2 were built using the Swiss-Model Workspace via Expasy web server programme [63] and molecular models were constructed with MacPyMOL software version 3.0 [64]. They possess side-by-side α-helices turning on the WXG motif, a feature shared by all WXG100 proteins [71]. Both structures have a flexible N-terminal segment that leads to nine turns of the α_1 chain extending to Trp44, and then a short hairpin bend links onto the α_2 chain with thirteen turns of the helix (Gly46 to Asn94). The alignment of the two models was nearly perfect (Fig. 7A and Fig. 7B).

Each protein sequence was blasted in NCBI BLASTp with default search parameters. Significant alignments were only found among the WXG100 family in the Firmicutes group. The top 10 hits were selected for CLUSTAL O multiple sequence alignments in SnapGene 5.0.8 (GSL Biotech LLC, USA). The multiple alignment showed that all the sequences possessed a conserved centrally located WXG motif and C-terminal secretion signal, *HxxxD/ExxhxxxH* (Fig. 7C). In this sequence, '*H*' stands for highly conserved hydrophobic and '*h*' for less conserved hydrophobic residues, '*x*' for any amino acid, and '*D/E*' for either aspartic or glutamic acids, respectively. In addition, they had non-hydrophobic inter-dimer interacting residues at positions 21 and 39, confirming that the two effector proteins and those in the NCBI BLASTp results belong to the monocistronic expressed *sag*EsxA-like subfamily of the WXG100 protein superfamily (Fig. 7C) [45,71]. The proteins Q81HA0 and Q81EA6 were henceforth renamed EsxA1 and EsxA2, respectively.

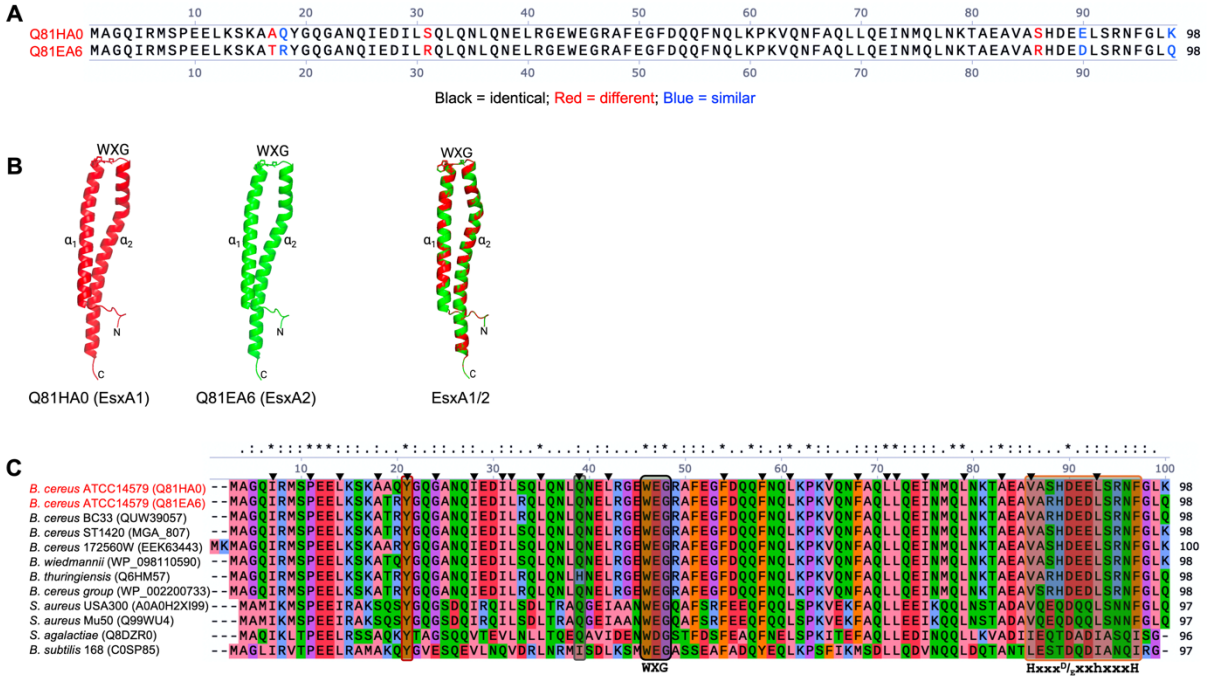

Figure 7. ESAT-6-like effector proteins in *B. cereus* are *sag*EsxA-like and conserved among Firmicutes.

A. The two ESAT-6-like proteins found in the WT secretome whose sequences are nearly identical, differing only in 3 amino acid residues at positions 17, 31 and 86.

B. Three-dimensional modelling structures of Q81HA0 (EsxA1) and Q81EA6 (EsxA2) show side-by-side α-helices linked with a hairpin bend formed by the centrally located WXG motif. Their superimposition (EsxA1/2) is a nearly perfect structural alignment for which the red and green colours indicate the alignment of EsxA1 and EsxA2, respectively.

C. CLUSTAL O alignments of the two WXG100 protein sequences, Q81HA0 and Q81EA6, found in the WT secretome and other firmicutes species. The alignment shows the centrally located WXG motif and a conserved C-terminal secretion signal with the *HxxxD/ExxhxxxH*. The four-helix bundle requires predominantly hydrophobic residues at a helix turn consisting of the heptad helix repeat shown by the up-side triangle (▼) on the aligned residues. All residues involved in the inter-dimer interactions are hydrophobic except two residues, position 21 and 39, which are unique to the *sag*EsxA-like subfamily.

esxA1 and *esxA2* are conserved among *B. cereus* strains

Genomic alignment of *S. aureus* USA300 and *B. cereus* ATCC14579 only identified one WXG100 encoding gene (Fig. 2). However, mass spectrometry analysis found two different WXG100 proteins (EsxA1 and EsxA2) (Fig. 6; Fig. 7). This suggested that two separate genes encoded EsxA1 and EsxA2. Thus, NCBI TBLASTn with *B. cereus* ATCC14579 as the database and EsxA1 and EsxA2 as query sequences confirmed that they were encoded by the genes *BC_RS04610* and *BC_RS10395,* respectively. Therefore, combining the genome alignment (Fig. 2) and mass spectrometry results (Fig. 6; Fig. 7), the genetic organization of *B. cereus* ATCC14579 the T7SSb was updated (Fig. 8). In the updated T7SS gene alignment, *BC_RS04610* and *BC*_RS10395 are renamed as *esxA1* and *esxA2*, respectively (Fig. 8). Further analysis among *B. cereus* strains found that *esxA1* and *esxA2* are conserved. The orphaned *esxA1* is located >1100 kb upstream of *esxA2*. Immediately downstream of *esxA1*, a gene encodes an LXG chaperon of the TIGR04197 protein family. In Figure 8, the TIGR04197 protein gene is written as *tigR*.

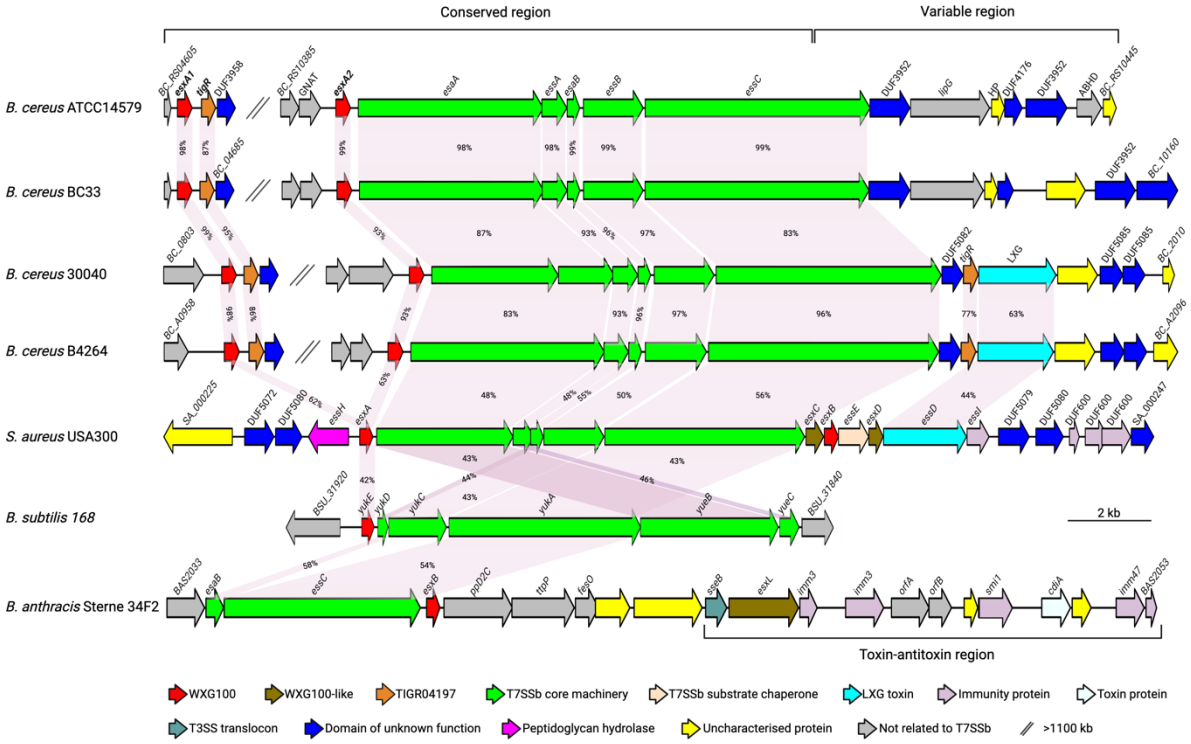

Figure 8. The T7SS effector genes, *esxA1* and *esxA2,* are conserved among *B. cereus* strains.

Note that *esxA1* is located more than 1100 kb upstream of the main T7SS gene cluster. Positioned in tandem with *esxA1* is *tigR,* which encodes the TIGR04197 protein, an LXG toxin chaperone in *S. intermedius*.

Discussion

The T7SS is characterized by an ATPase-driven secretion of approximately 100-residue helical proteins that contain a central WXG motif, with EsxA being the first identified T7SS substrate [72]. It is the major effector of the T7SS secretion system, essential for the virulence of pathogenic Gram-positive bacteria, such as *S. aureus* and *M. tuberculosis*. To date, no study had characterized the T7SSb in *B. cereus*, therefore, identifying the repertoire of the T7SSb in *B. cereus* in tandem with other closely related *Bacillus* species was the focus of this study.

Among the Gram-positive bacteria, the putative genomic organization of the *Bacillus* species' T7SS is said to be similar to that of *S. aureus* because both organisms belong to the phylum Firmicutes that possess a low guanine-cytosine ratio [30,73,74]. Thus, the methicillin-resistant *S. aureus* USA300, whose T7SSb has been well studied for its role in causing persistent infections and abscess formation [28,75], was selected for the T7SSb gene cluster homology analysis. The genome alignment of *S. aureus* and *B. cereus* ATCC14579 led to the identification of the five T7SSb core and one effector genes in *B. cereus* ATCC14579 arranged similarly on the same operon. The arrangement order from 5' to 3', there was *esxA* (effector), *essA*, *esaA*, *essB*, *esaB* and *essC* (core genes). Overall sequence homology was low, averaging below 52%, with the highest being *essC* at 56%. When the entire genome was further analysed for similar genes that could not be aligned in Mauve software (Darling lab, Australia) [53], another *esxA* gene was found at a distant locus upstream of the main T7SSb gene cluster. In addition, *a tigR* gene that encodes an LXG toxin (T7SS substrate) chaperon was located next to the orphaned *esxA,* which completed the putative T7SS gene cluster in *B. cereus* (Fig. 8).

Considering that diversity in T7SSb has been recorded in *S. aureus*, it was imperative to investigate the presence of similar heterogeneity among *B. cereus* strains. Homology analysis among *B. cereus* strains showed that the T7SSb gene cluster is conserved from the 5' end up to the proximal two-thirds of the *essC*. One-third on the 3' end of *essC* and the ensuing genes within the T7SS cluster showed variation among the strains. This could suggest that *B. cereus* strains have different *essC* alleles, each followed by a distinct set of genes. The less virulent *B. cereus* ATCC14579 and *B. cereus* BC33 did not possess virulence-encoding genes in the variable region. In contrast, the clinical isolates, *B. cereus* 30040 and *B. cereus* B4264, possess a second TIGR04197 protein and LXG toxin genes (Fig. 8). *B. cereus* 30040 was a major sequence type associated with nosocomial infections and bacteremia in Japan [7], while *B. cereus* B4264 was isolated from a case of fatal pneumonia in a male patient cultured from the blood and the pleural fluid in the USA [76]. The variable 3' end of the *essC* encodes the C-

terminal ATPase domain to which the substrate binds before secretion (Fig. 4). The EssC variants among Firmicutes are associated with unique effector repertoires, and, likely, a given EssC may only export substrates encoded by their cognate subtype. Studies on T7SS in *S. aureus* and *Listeria monocytogenes* strains have identified multiple *essC* alleles defined by downstream substrates. *S. aureus* and *L. monocytogenes* strains have been grouped into four and seven T7SSb variants, respectively [24,29,73]. *S. aureus* strains with *essC1* are clinical isolates, possessing *esxA*, *esxB*, *esxC*, *esxD,* and an LXG toxin gene followed by immunity genes, while the less pathogenic strains with *essC2* and *essC3,* the *esxD* is replaced by *tigR* [24,73]. In clinical isolates, a second TIGR04197 gene upstream of the LXG toxin gene could play a chaperone role in LXG toxin secretion by the T7SSb machinery similar to *S. intermedius* [47]. Our findings, and those of others, show that the T7SSb is very diverse between and within species, a reflection of virulence and implications for varied functions among the Firmicutes group.

By extension, similar analyses were conducted, comparing the T7SSb gene cluster in *B. subtilis* and *B. anthracis*. The T7SSb gene homologs were found in *B. subtilis,* though only possessing a single copy of *esxA* homolog, *yukE,* with 42% sequence identity. Many studies have shown that *B. cereus* is the closest relative to *B. anthracis* [52,77], however, the T7SSb repertoire is significantly different. *B. anthracis* possesses only two core genes, *esaB* and *essC,* followed by *esxB*. Downstream of these genes is followed by another WXG100-like protein gene, *esxL* (Fig. 4). Also, three more WXG100-like encoding genes were found at distant sites on the chromosome and another on pXO1. These genes were located in tandem (5' end) with immunity genes, implying that they encode toxins that form part of the TA system. Therefore, the WXG100-like proteins serve as T7SSb effectors as well as toxins in the TA system (Fig. 4). The cooperative relationship between the bacterial secretion system and the TA system has been established in *P. aeruginosa*. Hood *et al*. identified Tse2 and VgrG2b, T6SS effectors, are coregulated with the secretory apparatus and are toxin components of a toxin-immunity system that arrests the growth of prokaryotic and eukaryotic cells [69,78].

Furthermore, within the *B. anthracis* T7SSb gene cluster downstream of *essC*, there is an *sseB* gene that is typically part of the T3SS effectors. SseB is a secreted protein, part of the EspA superfamily, localized to the bacterial surface and forming part of the translocon of the T3SS encoded by the *Salmonella* pathogenicity island 2 [68,79,80]. This finding may imply that the deficiency in the typical T7SSb in *B. anthracis* may be compensated by SseB, although experimental evidence is required. Amongst the organisms analysed in this study, *B. anthracis* possesses the most divergent secretion system that future studies may propose as an

independent sub-type of the T7SS. Altogether, these findings point out that there is intraspecies and interspecies diversity in the T7SSb repertoire, and as such, inferences must be made with extreme caution.

Among the T7SSb structural proteins, EssC possesses the ATPase domain indispensable for the secretion of T7SSb-dependent effectors [18,48]. Therefore, to confirm that the identified T7SS was active and that the effector genes were expressed, a markerless *essC* deletion was made in *B. cereus* ATCC14579 for secretome comparison with the wild type. Through LC-MS/MS concatenated to a proteogenomic pipeline, we identified two EsxA proteins with 94% sequence identity in the wild-type culture supernatant and none in the *ΔessC* mutant. Protein sequence alignment showed that this pair belonged to the *sag*EsxA-like subfamily of the WXG100 superfamily. WXG100 proteins form dimeric complexes within the cytoplasm before secretion to increase solubility, and the driving force for the interdimer interactions is principally hydrophobic [71,81]. However, a pair of conserved and hydrophilic mutations among the proteins of the *sag*EsxA-like subfamily allows for interdimer hydrogen bonding. As a result, this conserved pair of mutations is seen as a fingerprint of homodimeric WXG100 proteins, which is in tandem with our finding of two nearly identical EsxA proteins (Fig. 7A).

In contrast, EsxA and EsxB in *S. aureus* and *M. tuberculosis* form heterodimers that only possess hydrophobic residues for interdimer interaction [71]. The genome analysis did not find an EsxB candidate among *B. cereus* strains, and similarly, *B. subtilis* T7SS lacks the EsxB homolog (Fig. 8) [50,51]. Among *Bacillus* species, EsxB has only been identified in *B. anthracis,* but it lacks EsxA [35]. The model structures show that EsxA1 and EsxA2 are helical hairpins, and their nearly perfect alignment supports interdimer interaction. Since both were found in the culture supernatant for the wild type, it may suggest that they were secreted as a dimer by the T7SSb machinery. Immunoblotting experiments can support this supposition once a specific *B. cereus* EsxA antibody is established. The graphic summary of the *B. cereus* T7SSb machinery with the secreted effectors is shown in Figure 9.

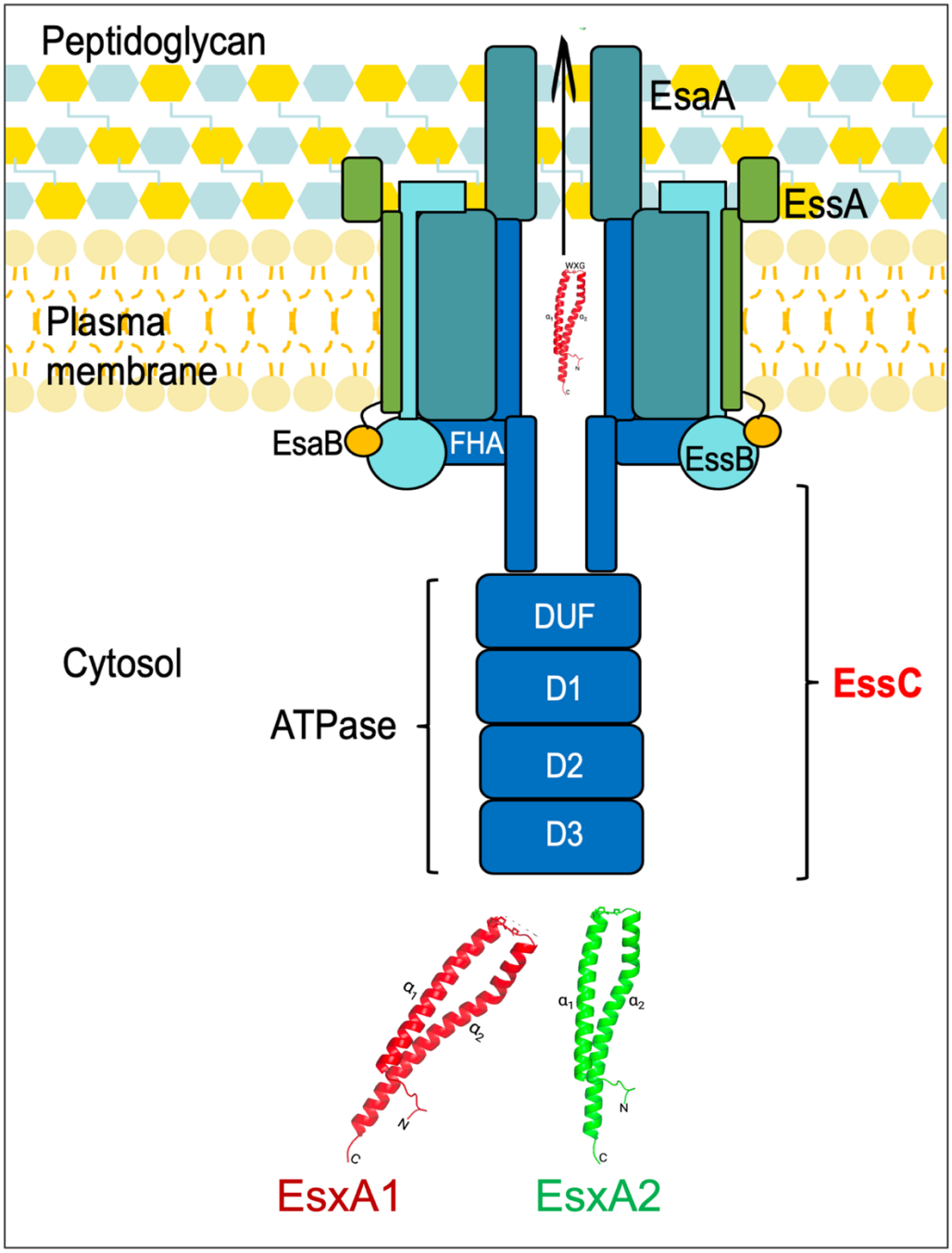

Figure 9. Graphic summary of the *B. cereus* T7SSb secretion machinery with its effector proteins (EsxA1 and EsxA2).

CHAPTER II

EsxA reveals a novel function in the sporulation of *Bacillus cereus* ATCC14579

Summary

Among the type VII secretion system (T7SS)-dependent effectors, the early secreted extracellular antigenic target (ESAT) type A (EsxA) has been extensively studied. Its roles in host-pathogen interactions are continuously being unravelled among Gram-positive bacteria of public health importance, however, its intrinsic functions remain elusive. Utilizing the *Bacillus cereus* type strain, *B. cereus* ATCC14579, markerless complete gene deletions encoding T7SS effectors and substrates were made that included *esxA1*, *esxA2*, *esxA1* and *esxA2*, *tigR* and *essC*. Next, the T7SS deletion mutants were investigated for phenotypic alterations resulting from mutations compared to the wild type. All these deletions did not affect the colony morphology, growth rates and biofilm production, however, the *ΔesxA1ΔesxA2* deletion significantly lost its ability to form mature spores efficiently. The *ΔesxA1ΔesxA2* mutant had a significantly lower viable spore count, reducing by almost 30% compared to the wild type and other T7SS mutants. Further, the *ΔesxA1ΔesxA2* strain delayed the onset of endospore formation, the early stage of spore formation, by 24 h. When complemented with either *esxA1* or *esxA2*, maximum sporulation rates similar to the wild type were restored, demonstrating that *esxA1* and *esxA2* worked redundantly and either was sufficient to restore the sporulation phenotype

These results indicate the intrinsic link between one of the virulence molecules, EsxA and the fitness of *B. cereus*. Further *in-silico* investigations hinted that EsxA may impact SpoIIIE functionality, a hexameric protein that translocates the chromosome from the mother cell into the endospore. The detailed molecular mechanisms of how EsxA regulates *B. cereus* sporulation and its biological significance in the *B. cereus* lifecycles, including the virulence, need further investigations

Introduction

A defining feature of many pathogenic Gram-positive bacteria is their ability to evade host immune defences, adapt to various environmental niches, and establish infection through specialized virulence mechanisms [82,83]. Among these, type VII secretion systems (T7SS) have emerged as key players in bacterial virulence, facilitating the export of specific proteins that enable interactions with host cells. One such protein, EsxA (ESAT-6), has attracted attention due to its unique role in mediating host-pathogen interactions in certain pathogenic Gram-positive bacteria [26,84–86].

Other known T7SS effectors include the 10 kDa culture filtrate protein named EsxB, and together with EsxA, they belong to the WXG100 protein superfamily. Additionally, WXG100-like effectors, EsxC and EsxD, have been identified in *S. aureus*, and the polymorphic LXG toxin among Firmicutes and their functions have been characterized [24–26]. Further, the TIGR04197 proteins have recently been linked to the T7SS based on phylogenetic profiling as a putative T7SS effector. Site-specific mutation in the TIGR04197 encoding gene abrogated LXG effector export, suggesting its significance in LXG effector secretion by the T7SSb apparatus in *Streptococcus intermedius* [47]. Among all these T7SS substrates, EsxA has been extensively studied, and its role in host-pathogen interactions is continuously being studied. For example, in *Mycobacterium tuberculosis*, EsxA disrupts the phagosomal membrane, facilitating the escape of bacteria from the phagosome into the host cell cytoplasm, where it can avoid degradation [19]. In *Staphylococcus aureus*, EsxA has been found to interfere with host cell apoptotic pathways to perpetuate infection [27] and is vital for abscess formation [28]. Within the bacteria itself, EsxA is required for the synthesis of EsxB, another T7SS-dependent effector. It also interacts with other multiple cellular proteins and stimulates several signal pathways within the bacteria [27,87–89]. Since EsxA is also found among non-pathogenic bacteria such as non-pathogenic *Mycobacterium* species and *Streptomyces scabies* [90,91], it suggests that it may have additional roles in bacterial fitness.

The fitness of *Bacillus cereus*, a spore-forming bacterium, is influenced by its ability to adapt to various environmental conditions and nutrient sources, which makes it a versatile organism capable of thriving in diverse environments. Key factors that contribute to the fitness of *B. cereus* include the ability to form spores and biofilms [92–94]. Formation of mature spores in *B. cereus* requires SpoIIIE, a protein crucial for DNA translocation during sporulation. SpoIIIE is indispensable for DNA translocation from the mother cell to the apically located forespore during sporulation. Formation of the asymmetric septum in *B. subtilis* results in the

enclosure of ~30% of the chromosome in the small forespore, and the rest is then actively translocated by SpoIIIE. It acts as a checkpoint that prevents septal membrane fusion until the completion of chromosome translocation via the aqueous DNA-conducting hexameric pore [95–98]. SpoIIIE belongs to the FtsK/SpoIIIE ATPase protein family with EssC, a membrane-bound protein with 'motor' functions central to the secretion of T7SS-dependent effectors. The observation of protomer contacts in the crystal structure of EssC is similar to the DNA translocase, suggesting a hexameric assembly for the FtsK/SpoIIIE proteins. In *Thermomonospora curvata*, in the absence of substrates, EssC is monomeric. Interaction with EsxB leads to dimerization of the EssC followed by higher order multimerization forming the hexameric pore required for successful secretion of the effectors [44,99]. EssC and SpoIIIE are multidomain with high homology in the substrate-binding C-terminal motor domain, and recruitment of multiple factors precedes multimerization [99–101]. However, whether an EssC substrate, EsxA in this case, can bind to another FtsK/SpoIIIE protein, such as SpoIIIE, and affect its function(s) is unknown.

Further, SpoVG is involved in sporulation as a pleiotropic regulatory factor in *B. subtilis* and *B. anthracis* sporulation [102,103]. In *Borrelia burgdorferi*, SpoVG is a highly conserved, site-specific DNA-binding protein that interacts with *esxA* and many other genes. Additionally, in *S. aureus*, transcription of *esxA* is controlled by a regulatory cascade involving downstream σ^B-dependent regulatory elements, including the SpoVG, staphylococcal accessory regulator SarA, and the ArlRS two-component system [104,105]. The pitfall is that *B. burgdorferi* and *S. aureus* are non-spore-forming organisms, thus, the impact of EsxA on sporulation could not be assessed in these species. Nevertheless, these findings suggest that EsxA may be involved in sporulation, other pathways, and bacterial homeostasis.

After identifying the genes that encode the putative T7SSb-dependent effectors, we conducted markerless full gene deletions to study the phenotypic characteristics after genomic alterations in *B. cereus* ATCC14579. Independent deletions of *esxA1* and *esxA2* resulted in strains with similar phenotypes and growth rates under normal and sporulation conditions. In contrast, the *ΔesxA1ΔesxA2* deletion resulted in significantly fewer viable spores and a slower sporulation process than the wild type.

Materials and methods

Bacterial strains and growth conditions

For routine culture, *B. cereus* strains were grown in Brain Heart Infusion (BHI) medium (Difco, USA) and *Escherichia coli* strains in Luria-Bertani (LB) medium (Difco, USA) at 37°C (shaking at 155 rpm for liquid cultures). Bacterial cultures for genetic manipulation were grown on media (BHI or LB) containing antibiotics at final concentrations of 250 μg/ml (*B. cereus*) or 100 μg/ml (*E. coli*) spectinomycin, 60 units/ml polymyxin, 50 μg/ml kanamycin, 100 μg/ml ampicillin and 10 μg/ml tetracycline. Cultures for sporulation assays were grown in 0.8% Nutrient Broth (Difco, USA), 1.2 % (wt/vol) $MgSO_4 \cdot 7H_2O$, 10% (wt/vol) KCl, 1 mM $Ca(NO_3)_2$, 0.01 mM $MnCl_2 \cdot 6H_2O$, and 1 μM $FeSO_4 \cdot 7H_2O$ (pH = 7.6) [106] under aerobic conditions at 30°C with shaking at 200 rpm.

Plasmid construction for gene deletion

Two plasmids were used to construct the *B. cereus ΔessC, ΔesxA1, ΔesxA2,* and *ΔtigR* strains, pRP1028 an *E. coli-Bacillus* shuttle vector and pRP1099 for facilitating homologous recombination. Briefly, pRP1028 is a temperature-sensitive replicon in *Bacillus* with an *I-Sce*I site, a sequence encoding the red fluorescent protein (RFP) and spectinomycin resistance gene. The facilitator plasmid pRP1099 contains genes for the *I-Sce*I enzyme under the control of a hybrid amylase promoter, green fluorescent protein (GFP) and kanamycin resistance. The bacterial strains and plasmids used in this study are shown in Table 5. The upstream (US) and downstream (DS) homologous arms of the target genes of *B. cereus* ATCC14579 were inserted into plasmid pRP1028 between the *Ban*II-*Sac*I and *Bsa*I sites to construct the derivative plasmids in Table 1 via Gibson Assembly (New England Biolabs, England) [55]. The US and DS fragments were generated via PCR using the forward and reverse primers indicated in Table 6. The recombinant plasmids were transformed into heat-shock competent *E. coli* 10β cells for amplification. Plasmid DNA was purified using the QIAprep Spin Miniprep Kit (Qiagen, Germany). Briefly, PCR was carried out to confirm the plasmids assemblies using KOD One Master Mix (TOYOBO, Japan) and diagnostic forward and reverse primers, pRP1028dx_F and pRP1028dx_R, respectively, whose sequences are shown in Table 6. The confirmed plasmids were subjected to sequencing PCR using a BigDye Terminator v3.1 Cycle Sequencing Kit (Applied Biosystems, USA) and subsequently sequenced using a 3130 Genetic Analyzer (Applied Biosystems, USA). The sequences were processed and aligned to the *B. cereus* ATCC14579 genome to confirm sequence correctness and orientation using SnapGene 5.0.8 software (GSL Biotech LLC, USA).

Construction of markerless deletion of T7SS genes in *B. cereus* ATCC14579

The allelic exchange system used in this study was developed based on the homing endonuclease I-SceI mediated markerless gene replacement method established in *B. anthracis* [57,107] with minor variations. We used the biparental mating method, eliminating the use of the helper strain (*E. coli* SS1827). We used *E. coli* SM10 and S17-1, which have *tra* genes encoding factors that can mobilize *oriT*-containing plasmids and integrate into chromosomes, thus making biparental mating possible. Each 50 µl aliquot of *E. coli* SM10 cells was independently transformed with recombinant shuttle vectors, pHKK100, pHKK102, pHKK104 or pYF07. The transformed *E. coli* SM10 cells (donor strain) were grown on LB agar with 100 µg/ml spectinomycin at 37°C overnight. *B. cereus* ATCC14579 (recipient strain) was also grown on BHI at 37°C overnight. Colony blobs of the donor and recipient strains were placed on BHI agar, mixed evenly, then spread on the entire plate, and incubated at room temperature for 24 h. The growth was swabbed onto BHI containing 250 µg/ml spectinomycin and 60 units/ml polymyxin B (BHI-Spe-Pmx) and incubated at room temperature for 48 h for conjugant *B. cereus* colony isolation. After twice passaging on BHI-Spe-Pmx incubated at 37°C overnight, pink-coloured *B. cereus* colonies were checked for red fluorescence using ImageQuant LAS 4000 Luminescent Image Analyzer (GE Healthcare, USA) with RFP Green (Epi-RGB) setting. Colonies that gave a positive fluorescent signal were swabbed together with *E. coli* S17-1 harbouring pRP1099 in BHI containing 50 µg/ml kanamycin and 60 units/ml polymyxin B and incubated at 37°C overnight. Spectinomycin-sensitive and RFP-negative *B. cereus* colonies were plated on BHI and incubated at 37°C overnight twice to lose the pRP1099 plasmid. Finally, the kanamycin-sensitive and GFP-negative colonies were confirmed to possess the desired deletion and sequence using specific diagnostic PCR shown in Table 6. To construct the *esxA* double mutant, *B. cereus ΔesxA1* (recipient) and *E. coli* SM10 harbouring pHKK102 (donor) were used and followed the same allelic exchange described above.

Construction of complimentary strains

To complement the *B. cereus ΔesxA1ΔesxA2* strain, a *GFP* plasmid, pGFP78, an *E. coli–B. subtilis* shuttle vector carrying a constitutive 78 promoter-controlled *GFP* gene was used. The pGFP78 plasmid DNA was purified using the Plasmid Midi Kit (Qiagen, Germany). The GFP open reading frame was removed from this vector by digestion with *Xba*I and *Hind*III (New England BioLabs, England) [108]. *B. cereus* ATCC14579 genome was used as a template to amplify *esxA1* and *esxA2* using specific primers in Table 6. PCR was carried out using KOD One Master Mix (TOYOBO, Japan), and the resulting amplicons and digested

pGFP78 *Δgfp* vector were purified using the MinElute Gel Extraction Kit (Qiagen, Germany). The *esxA1* and *esxA2* were independently ligated into the *Xba*I and *Hind*III sites of the pGFP78 *Δgfp* vector to generate pHKK114 and pHKK115 recombinant plasmids, respectively. The orientation and sequence of ligated plasmids were confirmed by sanger sequencing using specific complementation primers listed in Table 6. The recombinant plasmids were then transformed into *E. coli* 10β cells grown on LB agar with 10 µg/ml tetracycline for amplification. The plasmids were then purified using the QIAprep Spin Miniprep Kit (Qiagen, Germany). The recombinant plasmids were each electroporated into electrocompetent *B. cereus ΔesxA1ΔesxA2* using the Gene Pulser Xcell (BIO-RAD, USA) set at 1800 V, 25 µF, 200 Ω. Successful transformants were selected on BHI agar plates supplemented with 10 µg/ml tetracycline. In addition, the wild type and its isogenic *ΔesxA1ΔesxA2* were complemented with the original pGFP78 for growth in tetracycline. All these strains constructed here are listed in Table 5.

Table 5. Bacterial strains and plasmids used in this study.

Strain	Genotype or Description	Source
B. cereus		
ATCC14579	Wild type (WT)	[52]
	ΔessC (*essC* gene deleted mutant)	This study
	ΔesxA1 (*esxA1* gene deleted mutant)	This study
	ΔesxA2 (*esxA2* gene deleted mutant)	This study
	ΔtigR (*tigR* gene deleted mutant)	This study
	ΔesxA1ΔesxA2 (*esxA1* and *esxA2* genes deleted mutant)	This study
	ΔesxA1ΔesxA2+pGFP78::*esxA1* (*ΔesxA1ΔesxA2* mutant complimented with its native *esxA1* gene)	This study
	ΔesxA1ΔesxA2+pGFP78::*esxA2* (*ΔesxA1ΔesxA2* mutant complimented with its native *esxA2* gene)	This study
	ΔesxA1ΔesxA2+pGFP78 (*ΔesxA1ΔesxA2* mutant complimented with pGFP78 plasmid)	This study
	Wild type+pGFP78 (Wild type complimented with pGFP78 plasmid)	This study
30040 (ST1420)	Wild type clinical strain	[109]
E. coli		
SM10	*thi thr leu tonA lacY supE recA::RP4-2-Tc::Mu (Km)*	[56]
S17-1	*thi, pro, hsdR, RP4-2 Tc::Mu Km::Tn7 (Tp Sm)*	[56]
10β (C3019H)	*Δ(ara-leu) 7697 araD139 fhuA ΔlacX74 galK16 galE15 e14-ϕ80dlacZΔM15 recA1 relA1 endA1 nupG rpsL (StrR) rph spoT1 Δ(mrr-hsdRMS-mcrBC)*	New England BioLabs
Plasmids		
pRP1028	*Bacillus* and *E. coli* shuttle vector with *turbo-rfp* gene and an I-SceI recognition site; Spe^R	[57]
pRP1099	Vector with *turbo-AmCyan* and I-SceI genes; Kan^R	[57]
pGFP78	Shuttle vector for *Bacillus* and *E. coli* containing *gfp* gene and F78 promoter; Amp^R, Tet^R	[108]
pYF07	pRP1028 with upstream and downstream regions of *essC*	This study
pHKK100	pRP1028 with upstream and downstream regions of *esxA1*	This study
pHKK102	pRP1028 with upstream and downstream regions of *esxA2*	This study
pHKK104	pRP1028 with upstream and downstream regions of *tigR*	This study
pHKK114	pGFP78 *Δgfp* with *esxA1*	This study
pHKK115	pGFP78 *Δgfp* with *esxA2*	This study

Spe^R, Kan^R, Tet^R, and Amp^R stand for spectinomycin, kanamycin, tetracycline, and ampicillin resistance, respectively.

Table 6. Primers used in this study.

Primer name	Sequence (5'–3')[a]	Application
*essC*_US_F	cttgagctcctagcggccgcaagaaatgagaaattaagactacttcgg	For construction of *ΔessC mutant*
*essC*_US_R	ttaatttcagaattccatccgtgttcactgctc	
*essC*_DS_F	acacggatggaattctgaaattaaagaagaaagctaaggtg	
*essC*_DS_R	gtacaggtctccggccgctctgcgttaaatttatcctgtaatgtc	
*esxA1*_US_F	tcctagcgatgtgtgactatattggctgtttttatccaga	For construction of *ΔesxA1 mutant*
*esxA1*_US_R	gtatgacaatttttttcatttccccttttaatacataatgagcaaaatataaattgg	
*esxA1*_DS_F	gggaaatgaaaaaattgtcatactctatataacaagcatttcaaatgagc	
*esxA*_1_DS_R	tctccggccttaacttttgatttacttgattgatttgtttttcaatatcttgact	
*esxA2*_US_F	gcttgagcggatggatattaataggggaaaatacagactatttttct	For construction of *ΔesxA2 mutant*
*esxA2*_US_R	ctttttatctgtctattaaatccccccttaaaattaaaaaatagtaaaattaaccaataatca	
*esxA2*_DS_F	ggggatttaatagacagataaaaagaaatatataatttagccatgcaacc	
*esxA2*_DS_R	cgctaggattctgcctcagctttcaaatcct	
*tigR*_US_F	agcttgagcgttagtttggctgtagtagatattatcgttgcgaat	For construction of *ΔtigR mutant*
*tigR*_US_R	ggttgtcacacactcaaatcctttctctaattttcagaacatg	
*tigR*_DS_F	atttgagtgtgtgacaacctacgtaaaggtaaaatagtaagagga	
*tigR*_DS_R	gccgctaggactaatatttcttgttcaattacatctgtggaagc	
Dx_*esxA1*_F	ccaatttatattttgctcattatgtattaaagggg	PCR diagnosis of *esxA1* deletion
Dx_*esxA1*_R	ctttgaaattgtcccatcactcaaatcctttctc	
Dx_*tigR*_F	ggctcatttgattgcatgcccaac	PCR diagnosis of *tigR* deletion
Dx_*tigR*_R	cctgaatgtgaatcgcggattgatttcggtc	
Dx_*esxA2*_F	ggtttgcctttattttatagtagatttatagagtgtgc	PCR diagnosis of *esxA2* deletion
Dx_*esxA2*_R	cgactgcgagtctatctaatgaaagacttcgtatc	
*essC*_F	gctgtattggatgtataacgg	PCR diagnosis for *essC* deletion
*essC*_R	cgcttgtgttgtacttcc	
*esxA1*_F_C	gctctagacaatttatattttgctcattatgtattaaagggg	For *esxA1* complementation
*esxA1*_R_C	cccaagcttgctcatttgaaatgcttgttatatagagtatgac	
*esxA2*_F_C	gctctagaggtttgcctttattttatagtagatttatagagtgtgc	For *esxA2* complementation
*esxA2*_R_C	cccaagcttcgactgcgagtctatctaatgaaagacttcg	

[a] Restriction sites are underlined.

Hemolysis and proteolysis assessment

Assays for detecting the hemolysis and proteolysis capability of T7SS mutants were assessed using Blood Agar (BA) and Cereus Selective Agar (CSA), respectively. Commercially available AccuRate Sheep Blood Agar (Shimadzu, Japan) was used for hemolysis assay. Cereus Selective Agar (Base) supplemented with Polymyxin B sulphate 10 mg/l (Merck Millipore, Germany) and 10% [vol/vol] Egg Yolk Emulsion (Merck Millipore, Germany) was used for proteolysis assay. The WT and the T7SS mutants were grown in BHI broth at 37°C overnight with shaking and then diluted to OD_{600} = 0.1. Ten microliters of the diluted cultures were spotted on BA and CSA and incubated at 37°C for 16 h. The culture plates were then inspected for hemolysis and proteolysis.

Growth curve measurements

The *B. cereus* WT and its isogenic mutant strains generated in this study were grown in BHI for 16 h and then diluted to optical densities at 600 nm (OD_{600}) = 0.1. Ten technical replicates of diluted culture for each strain were added to the 96-well plate and monitored for growth by measuring OD_{600} every 10 min for 10 h using the Varioskan LUX Multimode Microplate Reader (Thermo Scientific, USA) at 37°C while shaking at 600 rpm. This experiment was done in three biological replicates. Growth rates were estimated from the slopes (log phase) obtained by fitting parametric models to the resulting data using GraphPad Prism version 8.4.3. The growth kinetics were also observed in LB and DSM cultures.

Biofilm formation assay

To analyse pellicle biofilm formation, the *B. cereus* strains were first grown in 3 ml of LB broth overnight at 37°C with shaking at 155 rpm. The cultures were then diluted to OD_{600} = 0.1 using LBGM (LB plus 1% [vol/vol] glycerol and 0.1 mM $MnSO_4$). LBGM is a novel biofilm-promoting medium among *Bacillus* species when grown at 30°C [110,111]. Twelve technical replicates of 180 µl of the diluted bacterial culture and control (LBGM) were added to each well of the 96-well plate. The plate was covered with a 96-peg lid supplied by the Biofilm formation Kit (Dojindo, Japan). The plate with cultures was incubated at 30°C for 72 h without shaking and was followed by washing and crystal violet staining steps as outlined in the Biofilm formation Kit (Dojindo, Japan). Biofilm formation was determined by measuring the optical densities at 595 nm (OD_{595}) using the Multiskan FC Microplate Photometer (Thermo Scientific, USA). The assay was replicated, and quantitative measures were

performed among the *B. cereus* strains after normalizing with the absorbance of uninoculated LBGM (negative control).

Determination of spore viability

The sporulation process observed under aerobic conditions in DSM has been shown to induce more robust sporulation capabilities in *B. cereus* [112]. *B. cereus* ATCC14579 and its five mutants were grown at 37°C in LB for 18 h and then diluted to OD_{600} = 0.1 in 10 ml DSM. The DSM culture was incubated under aerobic conditions at 30°C overnight with shaking at 200 rpm and then upscaled to 100 ml for up to 166 h until the fraction of spores/vegetative cells reached a maximum level [112]. One millilitre of aliquots of each sample was obtained every 12 h for measuring the OD and every 24 h for establishing the colony forming units (CFU) per ml. Serial dilutions of 100 µl culture and 900 µl of 1× phosphate buffered saline up to 10^6 dilutions were made. From the 10^6 dilutions, an aliquot of 500 µl was heat-treated at 80°C for 10 min to kill vegetative cells in the culture and then immediately put on ice [102,113] while the other 500 µl remained untreated. Four replicates of 20 µl of heat-treated and untreated aliquots were plated on LB and then incubated at 28°C for 14 h to enumerate the CFUs. This experiment was also done using pGFP78 complemented strains, in which DSM was supplemented with 10 µg/ml tetracycline. For each time interval, the mean CFU and sporulation ratios were obtained by CFU/ml = mean CFU ÷ (ml plated × dilution factor) and spore ratio = heat-treated mean CFU/ml ÷ untreated mean CFU/ml, respectively.

Assessment of sporulation rates

Aliquots of undiluted DSM cultures were obtained daily, stained using the classical Schaeffer-Fulton staining method [114] and then microscopically observed. In brief, 10 µl of the bacterial culture was smeared on the microscope slide and allowed to air dry. The bacteria smear was heat-fixed on the slide and stained with 0.5% (wt/vol) Malachite Green oxalate (Sigma-Aldrich, UK) salt over a 100°C water bath for 7 min. The excess Malachite Green stain was washed off using a gentle stream of tap water and air-drying, a counter stain, Safranin O 2.5% solution (Sigma-Aldrich, Japan) for 30 seconds. The excess stain was washed off using tap water, and the slides were left to dry. The slides were viewed by phase-contrast microscopy (×100, oil immersion; Nikon ELIPSE Ti, Nikon, Japan) with at least three visual fields examined to calculate the sporulation rate, and images were taken using a Nikon COOLPIX P310 camera. Sporulation rate = [mean spore count ÷ (mean spore count + mean vegetative cell count)] × 100%.

Statistical analyses

The statistical tests were performed using GraphPad Prism 8.4.3, as indicated in the figure legends, with *P* values < 0.05 considered significant. An ordinary unmatched one-way analysis of variance (ANOVA) with Dunnett's multiple comparisons test was applied for OD computations and CFU counts for the same time point. A matched two-way ANOVA was used for growth kinetics, daily OD, and sporulation ratio. All experiments were conducted with at least three biological and four technical replicates.

Protein structure modelling

The fasta files containing amino acid sequences for the WXG100 and FtsK/SpoIIIE proteins were uploaded into the Swiss-Model Workspace via Expasy web server program [63] to model the structure with default settings. The pdb output files were imported into MacPyMOL software version 3.0 [64] for further manipulations, analyses and construction of molecular model structures.

Results

Confirmation of T7SS gene deletions in *B. cereus*

The target genes for deletion were *esxA1*, *esxA2, tigR04197* (here shortened to *tigR*) and *essC,* which encode the T7SS effectors, a putative T7SS chaperon for LXG toxin in *S. intermedius* and the motor component of the T7SS, respectively. Utilizing the allelic exchange designed by Plaut and Stibitz [57], markerless whole gene deletions were made in *B. cereus* ATCC14579. The sizes of the deletions were 246 bp (*esxA1*), 321 bp (*esxA2*), 276 bp (*tigR*) and 4,498 bp (*essC*). In addition, both *esxA1* and *esxA2* were deleted to generate a double mutant bearing no T7SS effectors. The deletions were confirmed via PCR using specific diagnostic primers for each gene listed in Table 6. For the double mutant, in which the *B. cereus ΔesxA1* was used as the recipient strain for the *esxA2* mutant allele, multiplex PCR was done using diagnostic primers for *esxA1* and *esxA2* (Fig. 10). Colonies that possessed the desired deletion were preserved in BHI with 20% glycerol and stored at –80°C for downstream analyses.

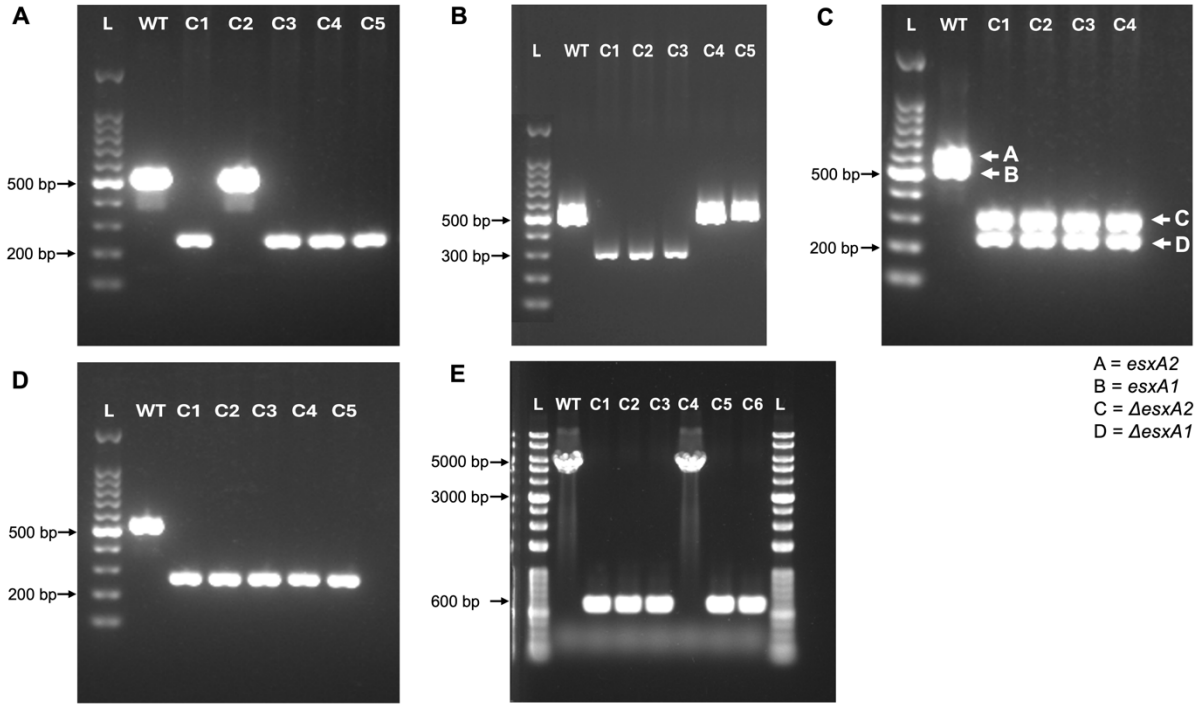

Figure 10. Colony PCR confirming deletion of *B. cereus* (WT) T7SS-related genes.

A. Confirmation of *esxA1* deletion and generation of *B. cereus ΔesxA1*. Sample colonies C1 and C3–C5 with about 250 bp products indicate deletion of *esxA1*. Colony C2 retained the wild-type allele.

B. Deletion of *esxA2* and generation of *B. cereus ΔesxA2*. Sample colonies C1–3 with approximately 300 bp desired. Colonies C4 and C5 reverted to the wild type.

C. Multiplex PCR for confirming the deletion of *esxA1* (~250 bp) and *esxA2* (~300 bp) and generation of *B. cereus ΔesxA1ΔesxA2*. All colonies possessed desired deletions.

D. Successful deletion of *tigR04197* (~280 bp) and generation of *B. cereus ΔtigR*. All colonies possessed desired deletions.

E. Confirmation of *essC* (~600 bp) deletion and generation of *B. cereus ΔessC.* Sample colonies C1–C3, C5 and C6 possessed the desired deletion, while colony C4 yielded reverted to the wild type.

Colony characteristics, hemolysis and proteolysis patterns

The phenotypic characteristics of the T7SSb deletion mutants obtained above were compared to the WT to assess the influence of the T7SSb. Some studies on the functional diversity of T7SS-dependent substrates have insinuated that secreted effectors may have multiple roles besides being just secreted virulence effectors [101,115,116]. Therefore, we screened the T7SSb gene-specific deletion mutants against the WT for morphotype changes. When checked for colony characteristics, the WT and the deletion mutant strains had similar colony size and morphology in BHI agar. All strains had colonies ranging 3-4 mm in diameter after 24 h growth at 37°C, cream-coloured, and spreading into the surrounding media with a granular surface (Fig. 11A). When 10 µl of the bacteria were spotted in triplicate on blood agar, they were all surrounded by a halo of hemolysis (Fig. 11B). Growth on Cereus Selective Agar base supplemented with 100 units/ml polymyxin B and 5% egg-yolk emulsion (Merk Millipore, Germany), induced egg-yolk precipitation by all strains seen as purple-coloured colonies and surrounding media (Fig. 11C). These findings indicate that deletions of the genes encoding the T7SS substrates (EsxA1, EsxA2 and TIGR04197) and the secretion system machinery (EssC) had not impact on colony morphology, hemolysis and proteolysis.

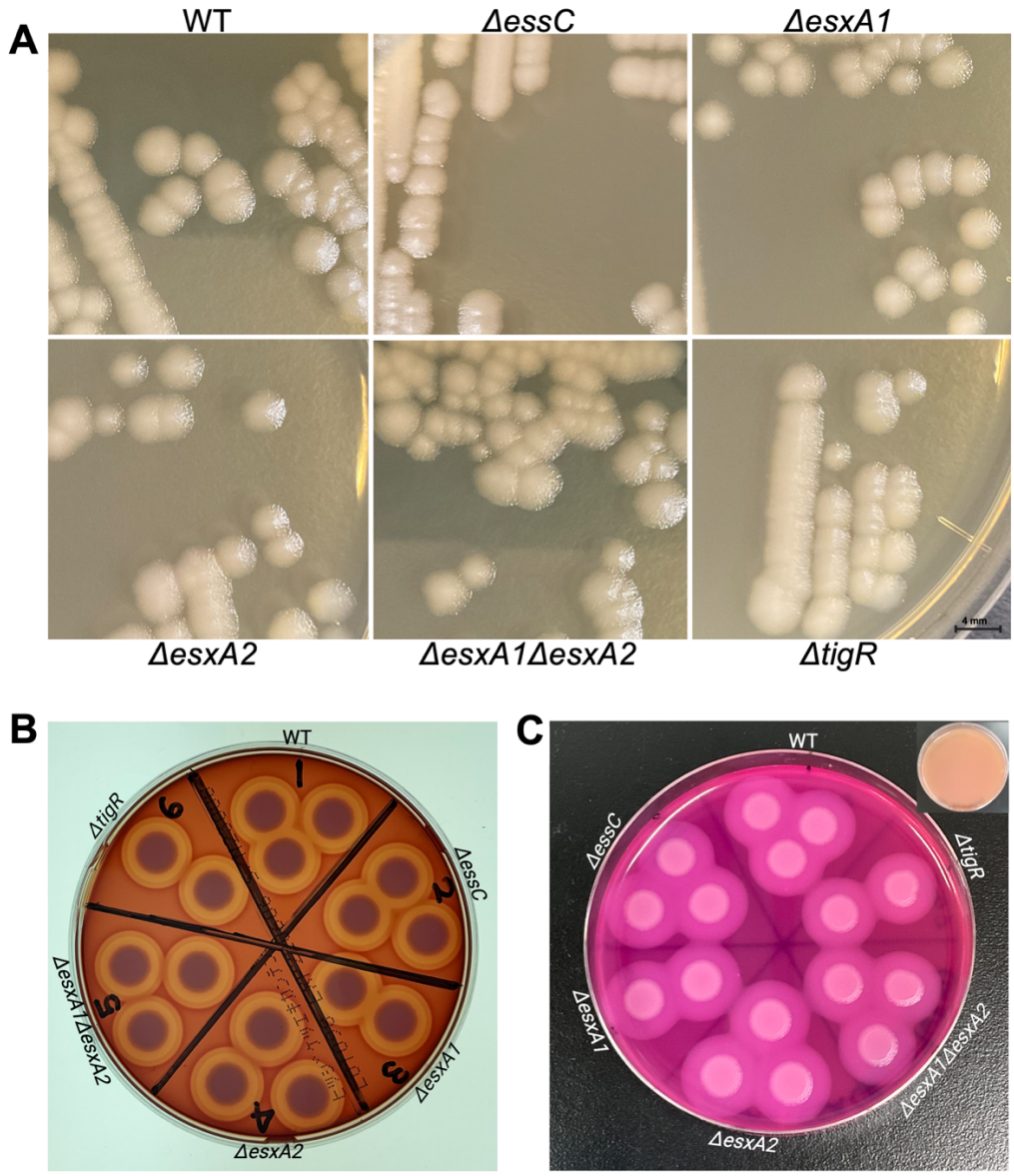

Figure 11. Morphological and biochemical characteristics of the strains.

A. Colony characteristics of the WT and its T7SS mutants cultured on BHI for 18 h at 37°C. The colonies are indistinguishable between strains, all being large (3 – 4 mm), cream-coloured, and spreading with a granular surface.

B. Strains on blood agar after 18 h incubation at 37°C, all strains exhibiting clear zones of hemolysis around the point of inoculation.

C. Growth on Cereus Selective Agar base supplemented with egg-yolk emulsion for 18 h at 37°C. All strains showed egg-yolk precipitation through proteolysis, seen as a colour change of the agar from deep peach (insert) to purple-red, especially the zones around the point of inoculation. Colonies are also purple-coloured because of proteolytic activity.

Growth kinetics among the strains in different culture media

Growth of the WT and the deletion mutants was observed as culture optical density over time at 37°C in BHI, LB and DSM. The growth curves shown in Figure 12 indicate that all deletion mutants followed a similar pattern to the WT from the lag phase to the stationary phase in different media used. The log phase, representing actual bacterial growth, for all strains (each strain: $n = 10$) ranged from 60 – 150 (BHI), 70 – 150 (LB), and 60 – 170 (DSM) min. Simple linear regression of the log phase showed no significant differences regardless of the media used. Since the slopes were not significantly different from each other, their pooled values of the log phases were 0.0058 ($R^2 = 0.995$), 0.0042 ($R^2 = 0.994$), 0.0030, and ($R^2 = 0.988$), in BHI, LB, and DSM, respectively. Thus, the gene deletions in this study did not alter the growth rate, suggesting T7SS does not play a role in the growth of *B. cereus*. The growth curves and their respective simple linear regression log phase slopes are shown in (Fig. 12).

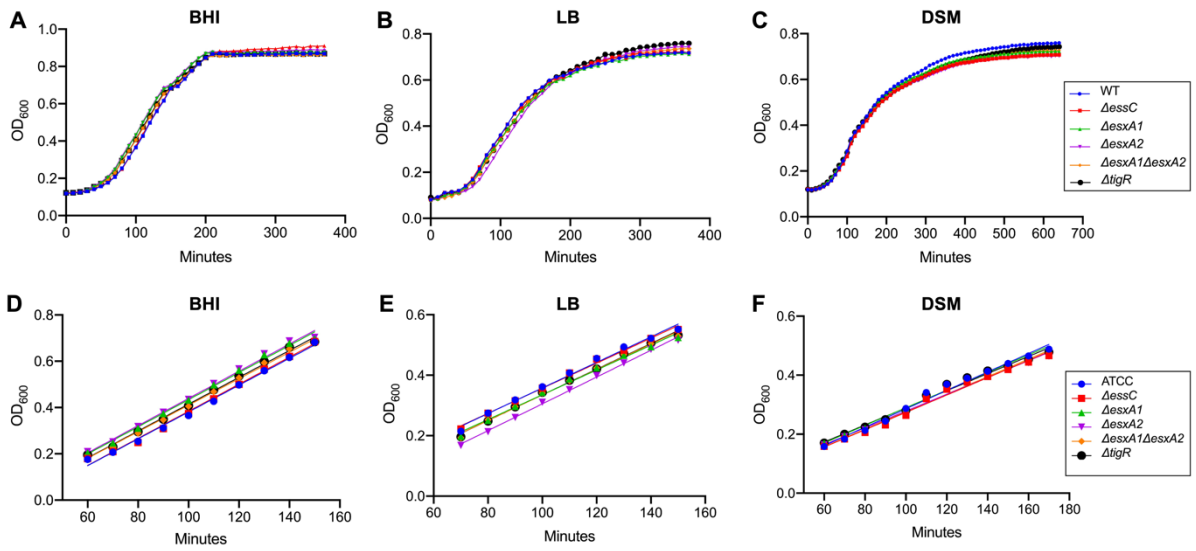

Figure 12. Growth of the WT and its deletion mutants in different media.

A – C. Growth curves of the WT, *ΔessC, ΔesxA1, ΔesxA2, ΔesxA1ΔesxA2*, and *ΔtigR* at 37°C in BHI **(A)**, LB **(B)** and DSM **(C)**. Bacterial growth was monitored by measuring the cell's optical density every 10 minutes.

D – F. Plots represent simple linear regression of the bacterial growth during the log phase in **(A)**, **(B)**, and **(C)**, respectively. There is no significant difference in the regression line slopes for each culture medium. The data represent the mean of 5 independent experiments performed in duplicates.

Biofilm formation ability

As shown in previous studies, biofilms formed by various *B. cereus* strains are diverse, with each strain having different abilities [111,117–119]. In a culture media that has been established to induce robust biofilms, there were no significant differences between the T7SS deletion mutants and their parent strain (WT) (Fig. 13A). This suggests that although EsxA may be involved in virulence, it plays no role in biofilm formation. *B. cereus* ATCC14579 is a laboratory-adapted strain, it is expected to form little biofilms that may not have been sufficient to detect differences with its T7SS isogenic mutants. To validate that the protocol induced biofilm formation, *B. cereus* 30040, a clinical strain that was isolated from patients and hospital equipment in Japan [7]. Compared to the *B. cereus* ATCC14579 and its mutants, the *B. cereus* 30040 produced almost ten-fold more biofilms on average. The heatmap shows results for the three biological and technical replicates (Fig. 13B). This finding confirmed that the conditions for biofilm formation were sufficient and that *B. cereus* ATCC14579 does not form robust biofilms.

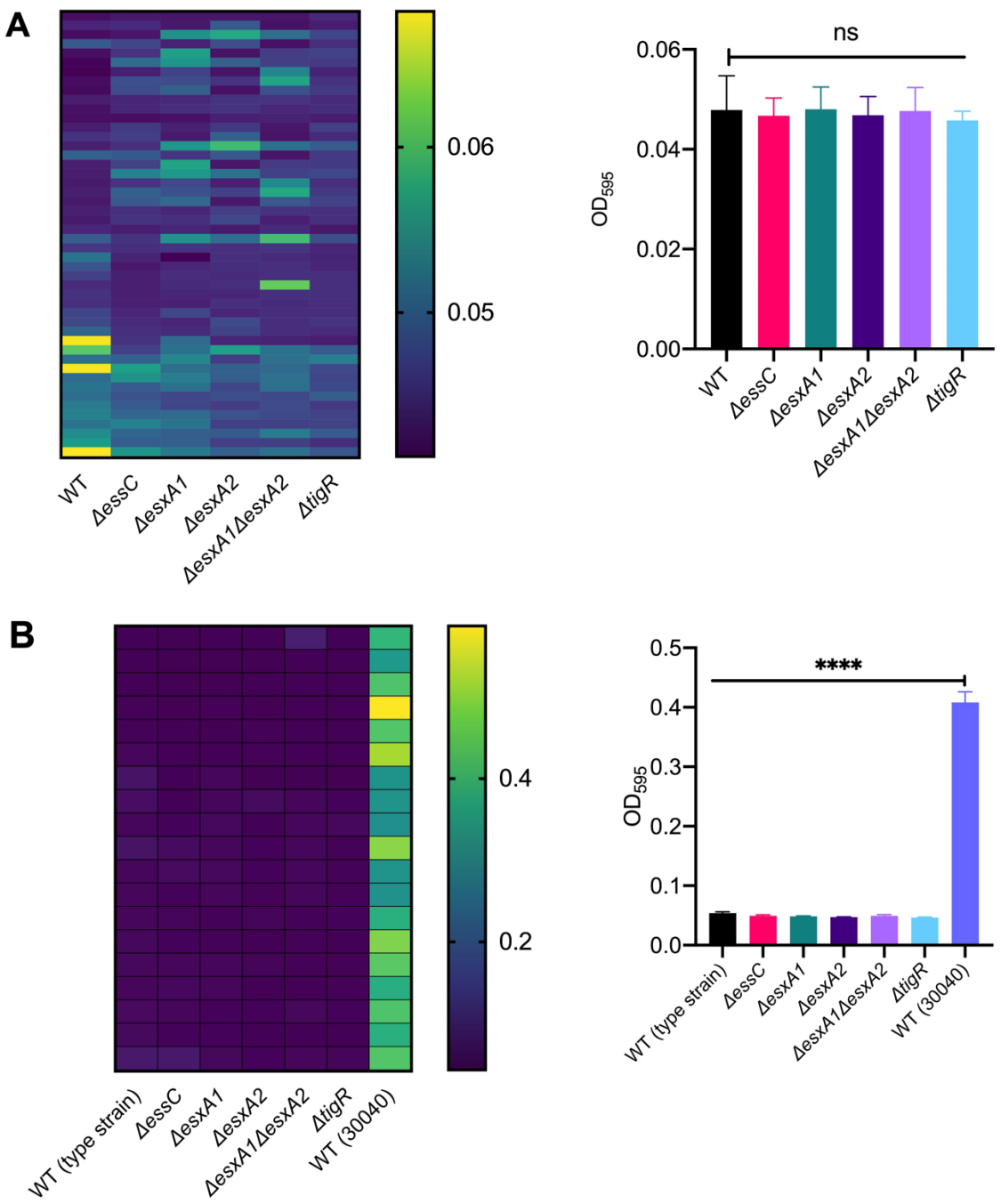

Figure 13. Biofilm formation of *B. cereus* strains used in this study.

A. Heatmap showing results for all three biological (n = 3) and technical replicates (n = 12). On average, biofilm production was similar among the strains, as seen in the bar graph.

B. With the addition of *B. cereus* 30040 to the experiment, the heatmap showed higher intensity for WT 30040 than the type strain and its mutants. The mean biofilm formation analyzed by Ordinary one-way ANOVA with Dunnett's test found a significant difference ****P < 0.0001.

Growth under sporulation conditions was impaired in *ΔesxA1ΔesxA2*

Under suitable growth conditions, the T7SS deletion mutants and the WT were indistinguishable; therefore, growth under nutritional stress and conditions that stimulated sporulation was checked next. Growth in DSM was monitored by measuring OD_{600} every 12 hours until a stable peak measurement. Figure 14A shows an exponential increase in OD in the first 36 h, followed by a sharp decrease in all strains except for *ΔesxA1ΔesxA2*, which exhibited a slow decline before becoming nearly constant after 120 h. At 120 h, *ΔesxA1ΔesxA2* had a significantly higher OD than other strains (Fig. 14B). The decrease in OD represented the sporulation process as mother cells lyse, releasing matures, a shift from the denser vegetative cells to smaller and lighter spores. Complementation of *esxA1esxA2* mutation with either *esxA1* or *esxA2* resulted in ODs comparable to the WT (Fig. 14C). The significantly higher OD in the *ΔesxA1ΔesxA2* mutant could be due to delayed autolysis by the mother cell required to release mature spores (Fig. 14D).

In assessing this hypothesis, the spore ratios were recorded from CFUs, and the sporulation rate was observed microscopically every 24 hours. From the onset of recording the CFU, *ΔesxA1ΔesxA2* had significantly fewer CFU at all time points of the entire experiment. The highest CFU/ml for the untreated and heat-treated cultures was observed after 120 h, at which their ratio was maximal for all the strains (Fig. 15A; Fig. 15B). Extended cultures did not yield different results, thus, the CFU data presented here were measured after 120 h of culture, which coincided with the stable OD (Fig. 14A; Fig. 15C). The *ΔesxA1ΔesxA2* mutant had a significantly lower spore ratio (~0.72), signifying fewer viable spores per ml. In contrast, *ΔesxA1, ΔesxA2, ΔessC and ΔtigR* mutants had spore ratio results comparable to the WT at all time points, peaking at approximately 0.96 after 120 h incubation (Fig. 15C; Fig. 16). There was a significant reduction in the mean CFU/ml for the *ΔesxA1ΔesxA2* mutant when heat treated, indicating the presence of vegetative cells after 120 h (Fig. 15B). Such a reduction was not observed in the WT and other deletion mutants. When complemented, maximum sporulation rates (97%) were restored in both *ΔesxA1ΔesxA2*+pGFP78::*esxA1* and *ΔesxA1ΔesxA2*+pGFP78::*esxA2* strains, demonstrating that *esxA1* and *esxA2* worked cooperatively and as either was sufficient to restore the sporulation phenotype (Fig. 15D – F). Our findings indicated that EsxA was essential for optimum spore formation in *B. cereus* ATCC14579.

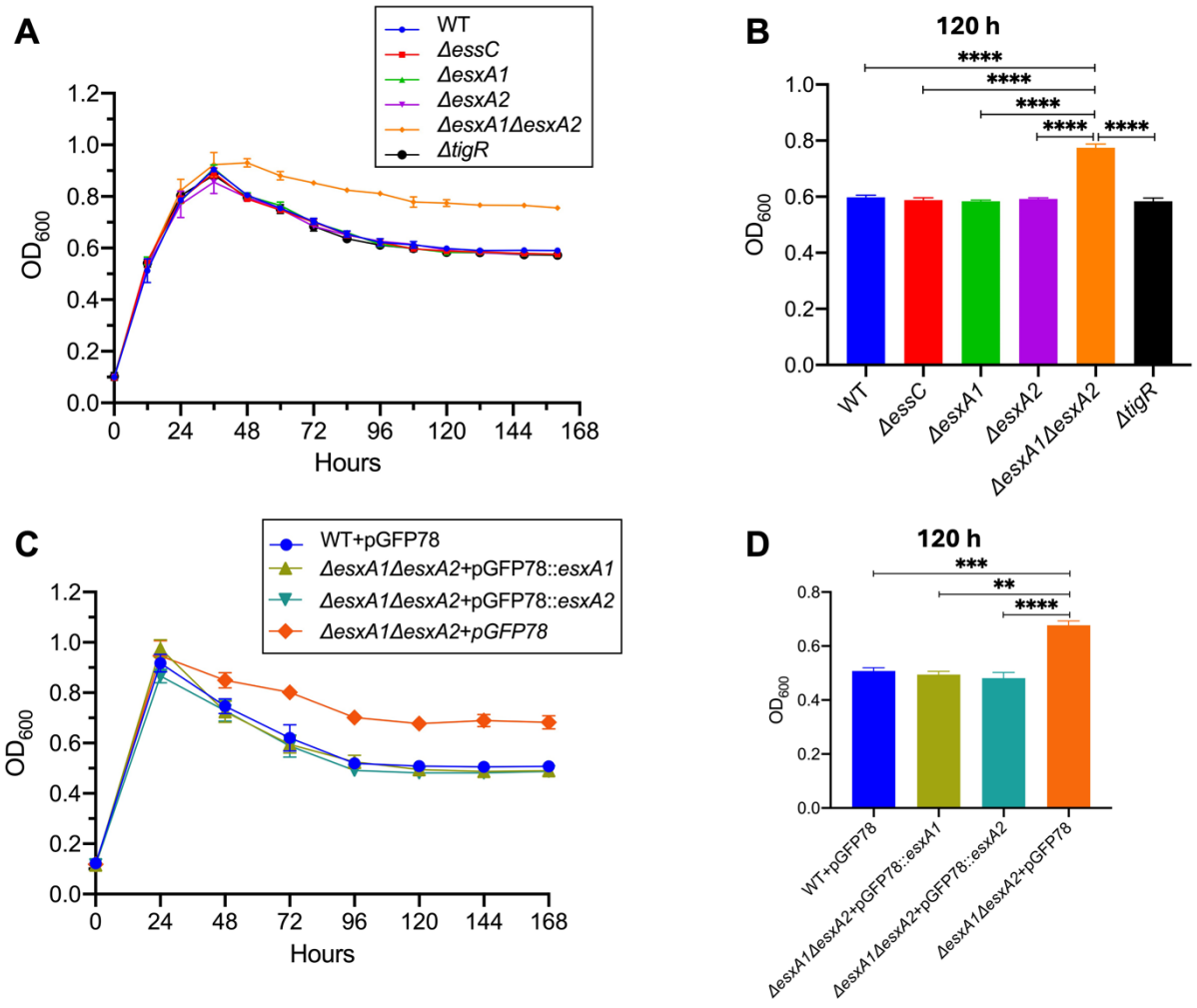

Figure 14. Growth in sporulation medium at 30°C.

A. The exponential phase lasted up to 36 h, at which point spore formation started. All strains but the *ΔesxA1ΔesxA2* had a slow decline in OD and did not reach the level of other T7SS deletion mutants and the wild type. The OD remained almost the same beyond 120 h.

B. Optical density measured at 120 h time point shows that *ΔesxA1ΔesxA2* had significantly higher optical density. Statistical significance was calculated by Ordinary one-way ANOVA with Dunnett's test, ****P < 0.0001.

C. Complementation of the *ΔesxA1ΔesxA2* strain with either *esxA1* or *esxA2* exhibited a similar growth kinetic to the wild type. Their rate of reduction of the optical density beyond the exponential phase was identical to the wild type, while *ΔesxA1ΔesxA2* maintained the slow decline in the optical density.

D. Optical density for complemented strains measured at 120 h time point with the uncomplemented *ΔesxA1ΔesxA2*+pGPF78 maintaining a significantly higher optical density. Statistical significance was calculated by Ordinary one-way ANOVA with Dunnett's test, ***P < 0.0003; ****P < 0.0001.

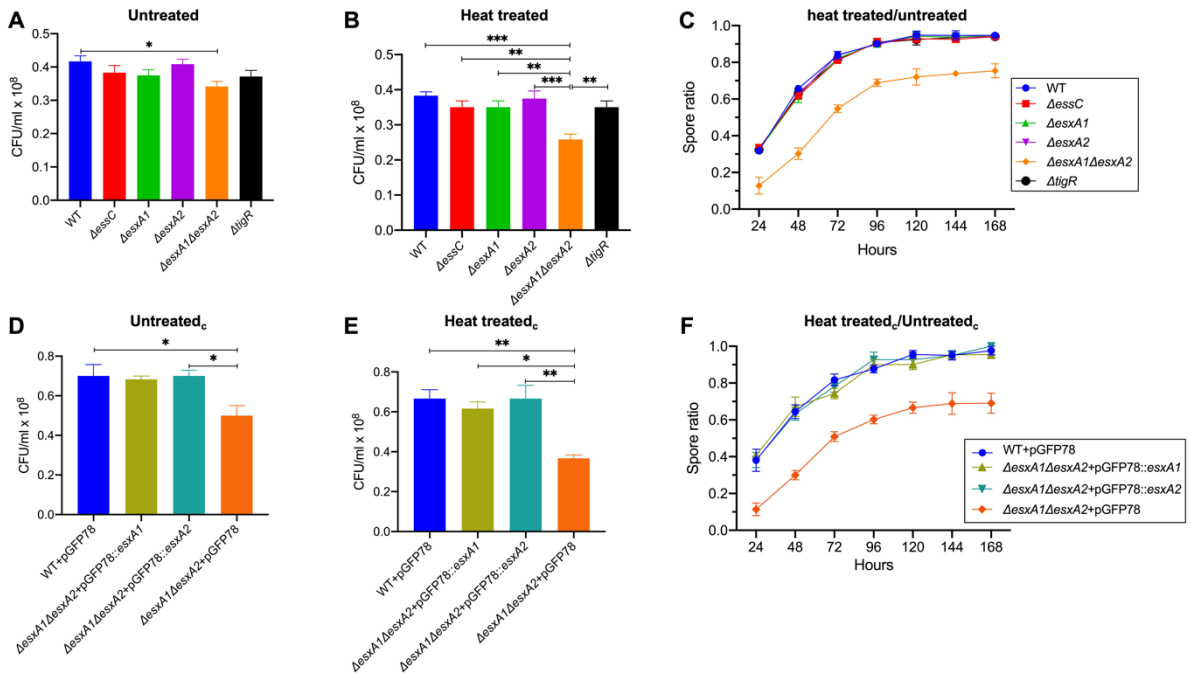

Figure 15. Colony-forming units per millilitre and sporulation rates of experiment strains cultured in DSM at 30°C.

A. The mean CFU/ml for untreated (vegetative cells + spores) for the *ΔesxA1ΔesxA2* was significantly lower than the wild type after 120 h incubation.

B. Heat treatment that killed vegetative cells resulted in further significantly lower CFU counts for *ΔesxA1ΔesxA2* compared to the rest of the strains after 120 h of culture.

C. Time course sporulation rates were calculated as the ratio of CFUs/ml for heat-treated and untreated WT and its mutants. The *ΔesxA1ΔesxA2* had a significantly slower and deficient sporulation rate than all other strains in this study.

D. Complementation of the *ΔesxA1ΔesxA2* strain with either *esxA1* (*ΔesxA1ΔesxA2*+pGFP78::*esxA1*) or *esxA2* (*ΔesxA1ΔesxA2*+pGFP78::*esxA2*) resulted in restored CFUs to levels of the wild type.

E. Heat treatment of the complemented strains had comparable CFUs to the wild type, but the uncomplemented *ΔesxA1ΔesxA2*+pGFP78 had significantly fewer CFU/ml.

F. Time course sporulation rates for complemented strains and their mean CFUs/ml for the untreated (D) and heat-treated cultures (E).

Statistical significance was calculated using Ordinary one-way ANOVA with Dunnett's multiple comparisons test, *P < 0.0382; **P < 0.0093; ***P < 0.006 for three independent experiments.

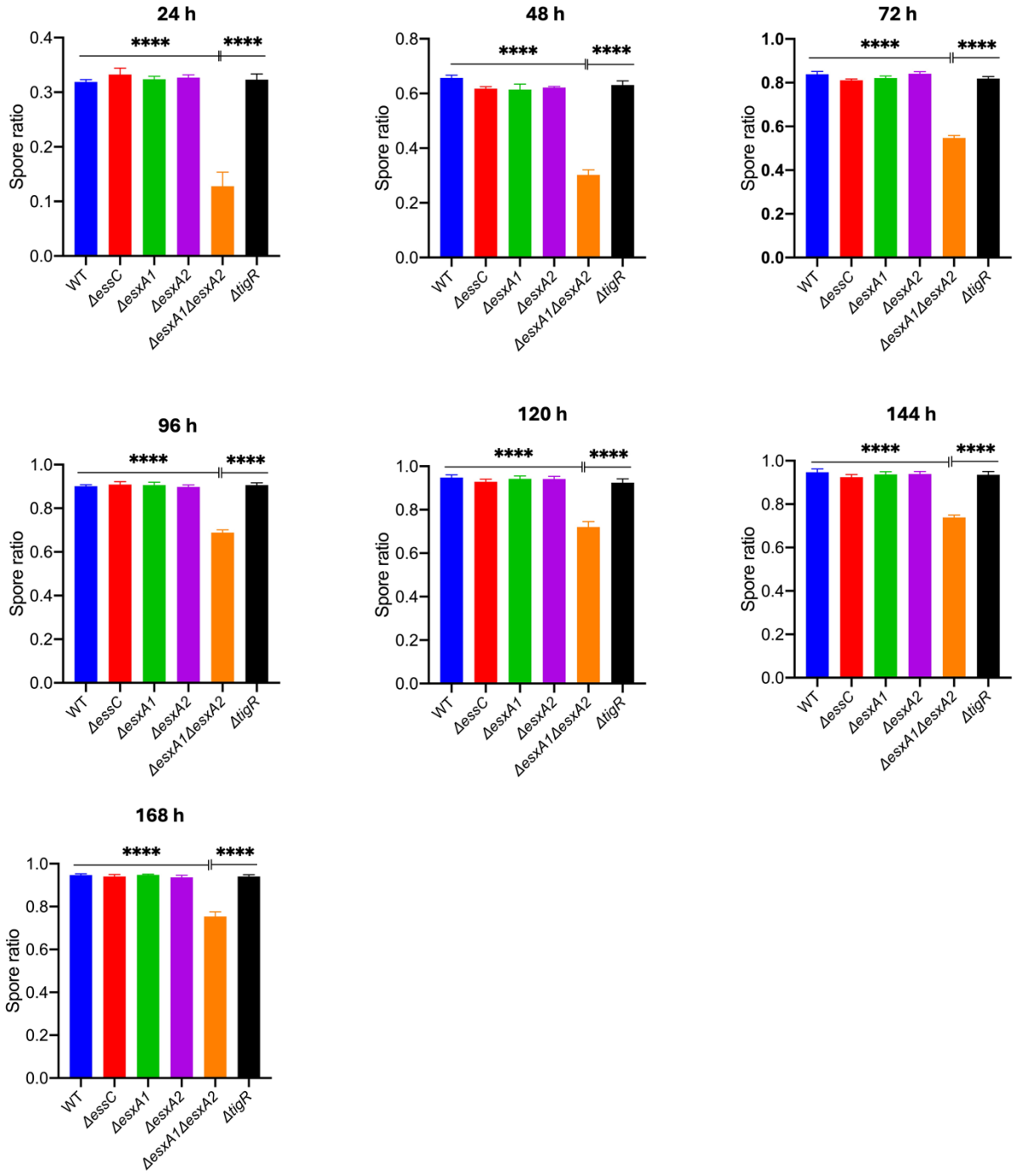

Figure 16. Calculated spore ratios recorded every 24 hours.

The *ΔesxA1ΔesxA2* produced significantly fewer viable spores at all sampled time points than the WT. All strains had their maximum spore ratios after 120 h of incubation, where the WT and other deletion mutants reached 0.96 except for the *ΔesxA1ΔesxA2,* which could only reach 0.72 on average. Statistical significance was calculated using Ordinary one-way ANOVA with Dunnett's multiple comparisons test, ****P < 0.0001 for three independent experiments.

EsxA is essential for optimum sporulation in *B. cereus* ATCC14579

The *ΔesxA1ΔesxA2* mutant was found to have a significantly higher OD but a significantly lower CFU/ml, fewer spores, and a lower sporulation ratio. Microscopy of the Schaeffer-Fulton method-stained cultures was conducted to evaluate the delayed mother cell autolysis hypothesis. Phase contrast microscopy showed early evidence of sporulation in the majority (> 80%) of the WT cells generating endospores within 24 h compared to *ΔesxA1ΔesxA2* with less than 10%. The *ΔesxA1ΔesxA2* mutant endospores poorly took up malachite green stain at this time, suggesting fewer endospores (Fig. 17). After culturing for 48 h, WT released a mass of mature spores, but *ΔesxA1ΔesxA2* had a few mature spores, and almost 55% of the cells had endospores. Further, the *ΔesxA1ΔesxA2* mutant had vegetative cells beyond 96 h that maintained the chaining phenotype typical of *Bacillus* species. The presence of vegetative cells accounted for the significantly higher OD and a reduced sporulation rate, whose peak was 72%. In contrast, at 96 h, the WT sporulation rate almost reached 100%. These findings ruled out our hypothesis, assuming that delayed autolysis of mother cells with mature endospores caused a significantly higher OD and lower spore ratio, but rather, due to an inefficient sporulation process altogether. Again, complementation of *ΔesxA1ΔesxA2* with either *esxA1* or *esxA2* reversed the sporulation deficiency to levels of the WT (Fig. 18). Therefore, it was concluded that the two EsxA proteins work cooperatively and play a significant role in the optimal sporulation of *B. cereus* ATCC14579.

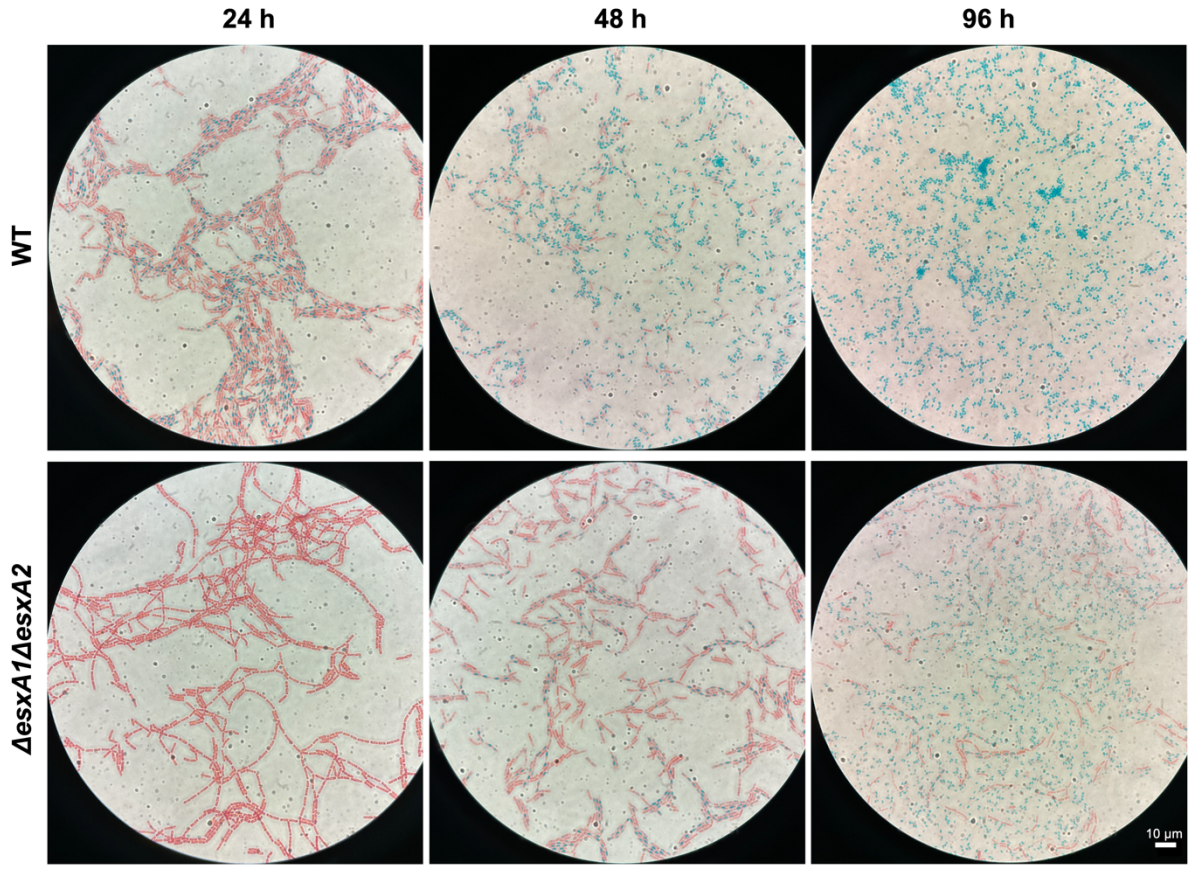

Figure 17. The spore staining results of *B. cereus* ATCC14579 and *ΔesxA1ΔesxA2*.

When stained with malachite green and safranin O, matured spores and endospores are stained blue, and vegetative cells are stained red. Within 24 h, more than 80% of the WT cells had formed endospores (blue cytoplasm), but less than 10% in *ΔesxA1ΔesxA2* cells, which are immature (forespores) and poorly take up the malachite green stain. After 48 h, the WT underwent 66% sporulation on average, while the mutant had approximately 45% endospores and 20% mature spores. Beyond 96 h, the WT had almost all cells sporulated, but *ΔesxA1ΔesxA2* still had vegetative cells (28%) occurring in chains.

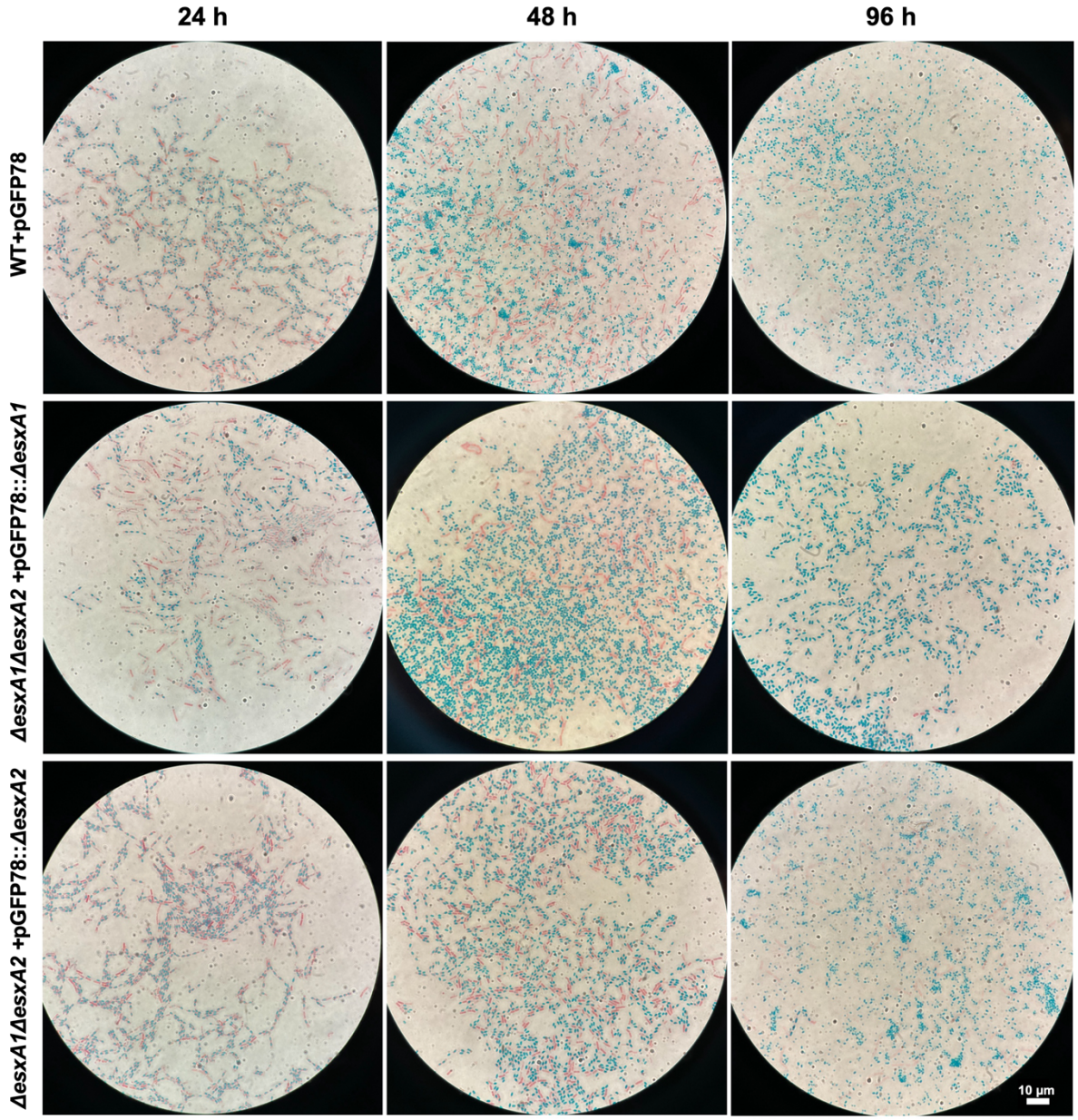

Figure 18. The spore staining results of complementary strains.

Complementation of *ΔesxA1ΔesxA2* with either pGFP78::*esxA1* or pGFP78::*esxA2* restored sporulation rates to levels of the WT. Spores and endospores are stained blue, while vegetative cells are red. The WT was also complemented with pGFP78 to allow growth of all complemented strains under similar conditions in 10 µg/ml tetracycline.

Discussion

In this study, the type strain *B. cereus* ATCC14579 was used to evaluate the influence that its T7SSb may have on phenotypic characteristics and fitness. Full gene deletions encoding the T7SSb effectors (EsxA1, EsxA2), substrate (TIGR04197), and the motor component, EssC, were made for the evaluation compared to the wild type. Among the mutants, the strain in which both *esxA1* and *esxA2* were deleted exhibited significantly fewer viable spores, and the sporulation rate was significantly slower, too. These results indicate the intrinsic link between one of the virulence machineries, the T7SSb, and the fitness of *B. cereus*, a common environmental zoonotic pathogen.

Studies on T7SS continue to focus on its involvement in host-immune interactions and niche adaptations. However, given the inter and intraspecies variations in the T7SS repertoire [29,30], unravelling the intrinsic roles of the T7SS is paramount. The information gathered could provide insights into the pathways they are involved in and serve as new targets for antimicrobials in the wake of emerging drug-resistant bacteria [31]. Bacterial secretion systems have now become an attractive target for developing antibacterials as they are essential in the pathogenesis of many bacteria [120,121]. Here, genomic deletions were made in the genes encoding the T7SS-dependent effector (*esxA),* a chaperone for LXG toxin (*tigR*) and the ATPase domain of the T7SS (*essC*). In *B. cereus* ATCC14579, two genes located at distant loci encode respective EsxAs, which in this study are designated *esxA1* and *esxA2*. Therefore, strains with independent deletions of *esxA1*, *esxA2* and both genes were also generated (Fig. 10). After confirming the success of the genomic alterations, their phenotypic characteristics were investigated. Phenotypically, their colonies were cream-coloured on BHI and, on average, measured 3–4 mm in size, finding that are typical of *B. cereus*. The T7SS mutants had a morphotype similar to the wild type. In addition to their ability to produce and secrete hemolytic and proteolytic enzymes, a feature common to *B. cereus*, the mutant strains also expressed these abilities. Their growth rates under optimal nutrition and temperature were also comparable to the wild type in different culture media. This meant the deletions made had no impact on their growth kinetics.

When the strains were tested for spore-forming ability under sporulation-inducing conditions, the strain lacking both *esxA* genes, *ΔesxA1ΔesxA2*, exhibited a delayed and significantly reduced ability to form viable spores. Heat treatment of the *ΔesxA1ΔesxA2* spore culture significantly diminished the number of viable spores enumerated as CFUs. It was evident from the fraction of the spores that *ΔesxA1ΔesxA2* had significantly fewer viable spores

throughout the culture period compared to the WT and other mutants (Fig. 15). Generally, a higher bacterial culture optical density is assumed to translate to a higher CFU count, however, our findings for the *ΔesxA1ΔesxA2* defied that notion. Despite having a significantly higher OD_{600} (Fig. 14), *ΔesxA1ΔesxA2* consistently produced fewer viable spores than wild type and other T7SS deletion mutants. Phase contrast microscopy showed no evident aberrations in cell and spore morphologies, only a delayed and reduced sporulation in *ΔesxA1ΔesxA2,* which agreed with the CFU results. Overall, the *ΔesxA1ΔesxA2* culture still had vegetative cells reaching 28% on average of any microscopic field viewed (Fig. 17). When complemented with either *esxA1* or *esxA2*, the mutant fully recovered the spore formation ability (Fig. 18), suggesting the cooperative function of the EsxA1 and EsxA2 and their involvement in sporulation of *B. cereus*.

In contrast, the *ΔessC* mutant, in which we found that EsxA was not secreted, had similar sporulation results as the WT. This indicated that EsxA did not affect sporulation after being secreted, but its expression within the cell was necessary to maintain optimum sporulation. Thus*, ΔesxA1*, *ΔesxA2,* and *ΔtigR* sporulation phenotypes were unaffected. These findings confirmed that EsxA is not only a secreted effector protein but has additional roles within the milieu and, in this case, sporulation. Other studies have also indicated that T7SS-dependent effectors have additional roles within the bacterium. Fyans *et al*. [91] reported that the ESX/type VII secretion system modulated development but not virulence in *Streptomyces scabies*, a plant pathogen. Specifically, the EsxA and EsxB mutants had abnormal spore chains and exhibited resistance to lysis by the *Streptomyces*-specific phage ϕC31. Similarly, deletion of the EsxAB operon in *Streptomyces coelicolor* resulted in irregular-sized pre-spore compartments with corresponding aberrant DNA contents. The EsxAB heterodimer was proposed to control the coordination of cell division with the segregation of nucleoids, most probably through interaction with other factors that regulate nucleoid condensation [122]. However, in *B. cereus*, growth, size, and morphology of the colonies and cells of the *ΔesxA1ΔesxA2* mutant were unaffected. The T7SS-mediated phenotypes seemingly depend on T7SS subtype-specific regulation that may affect several signal pathways [27,87–89]. Thus, T7SS substrates possess diverse species-specific cellular functions and can modulate interactions between bacteria and eukaryotic cells [115].

This finding is interesting, given that spores are a significant component of bacterial biofilms that are an important factor in treating and controlling biofilm-producing bacterial infection and contamination. *B. cereus* biofilms are highly resistant to disinfectants, and up to 90% of biofilm cells are spores in matured biofilms [123,124]. This would explain why *B.*

cereus 30040 was able to survive on hospital equipment and surfaces in Japanese hospitals [7] as it can form biofilms more efficiently than the type strain and its T7SS mutants (Fig. 13B). While the T7SS mutants produced similar biofilms to the wild type, the meagre amounts may not have been sufficient to detect the difference. Therefore, an understanding of the synergy between biofilm formation and sporulation could be better evaluated using *B. cereus* 30040 *ΔesxA1ΔesxA2*.

One of the possible mechanisms of how EsxA plays an important role in the sporulation in *B. cereus* is that EsxA may interact with SpoIIIE and enhance its functionality. The protein-protein interaction analysis using STRING [125] (https://string-db.org) showed that YukE, an EsxA from *B. subtilis*, may interact with SpoIIIE (Fig. 19A). SpoIIIE is a DNA translocase that drives up to 70% of the chromosome across the forespore septum before endospore formation [96,126]. Since *B. cereus* EsxA proteins could not be analyzed in the STRING database, and the sporulation pathway is well understood in *B. subtilis* [127–130], the prediction data was obtained using *B. subtilis* protein information. Although the amino acid sequences of EsxA and YukE have low homology, the superimposition of their predicted structures was nearly perfect (Fig. 19B). Further, the SpoIIIE proteins from *B. cereus* and *B. subtilis* were predicted to possess a high structural homology (Fig. 19C), therefore, it can be speculated that EsxA-SpoIIIE interaction may occur, and it impacts sporulation in *B. cereus.* In addition, the ATPase domain of *B. cereus* SpoIIIE possesses a high structural similarity with the ATPase domain of EssC protein, as Mietrach *et al*. revealed previously [18]. Just like EsxB binds to EssC in *S. aureus*, causing the multimerization of EssC to form the hexameric secretion pore [99,131], SpoIIIE also forms a hexameric pore to pass DNA [100,101]. Hence, in the absence of EsxB in *B. cereus* ATCC14679, it is more likely that EsxA may promote EssC and SpoIIIE multimerization. Previously, it was observed in *S. coelicolor* that the loss of function of the EsxAB heterodimer impacted the coordination of cell division and the segregation of nucleoids. But even multiple gene mutations involved in the coordination of nucleoid condensation and segregation, including *ftsK*, also resulted in similar septation aberrations, implying it depends on several overlapping and partially redundant functions [122]. Similarly, in *B. cereus* ATCC14579, loss of EsxA1 and EsxA2 may be impacting the sporulation function of SpoIIIE, an FtsK protein. Thus, without EsxA in the *ΔesxA1ΔesxA2* mutant, SpoIIIE translocation of DNA may have been inefficient, resulting in delayed sporulation and fewer mature spores in *B. cereus* ATCC14579. On the other hand, EsxA might have a completely different novel mechanism affecting sporulation, which regulates the function or transcription of sporulation-related genes. The detailed molecular mechanisms of how EsxA regulates *B. cereus* sporulation

and its biological significance in the *B. cereus* lifecycles, including the virulence, need to be addressed in future studies.

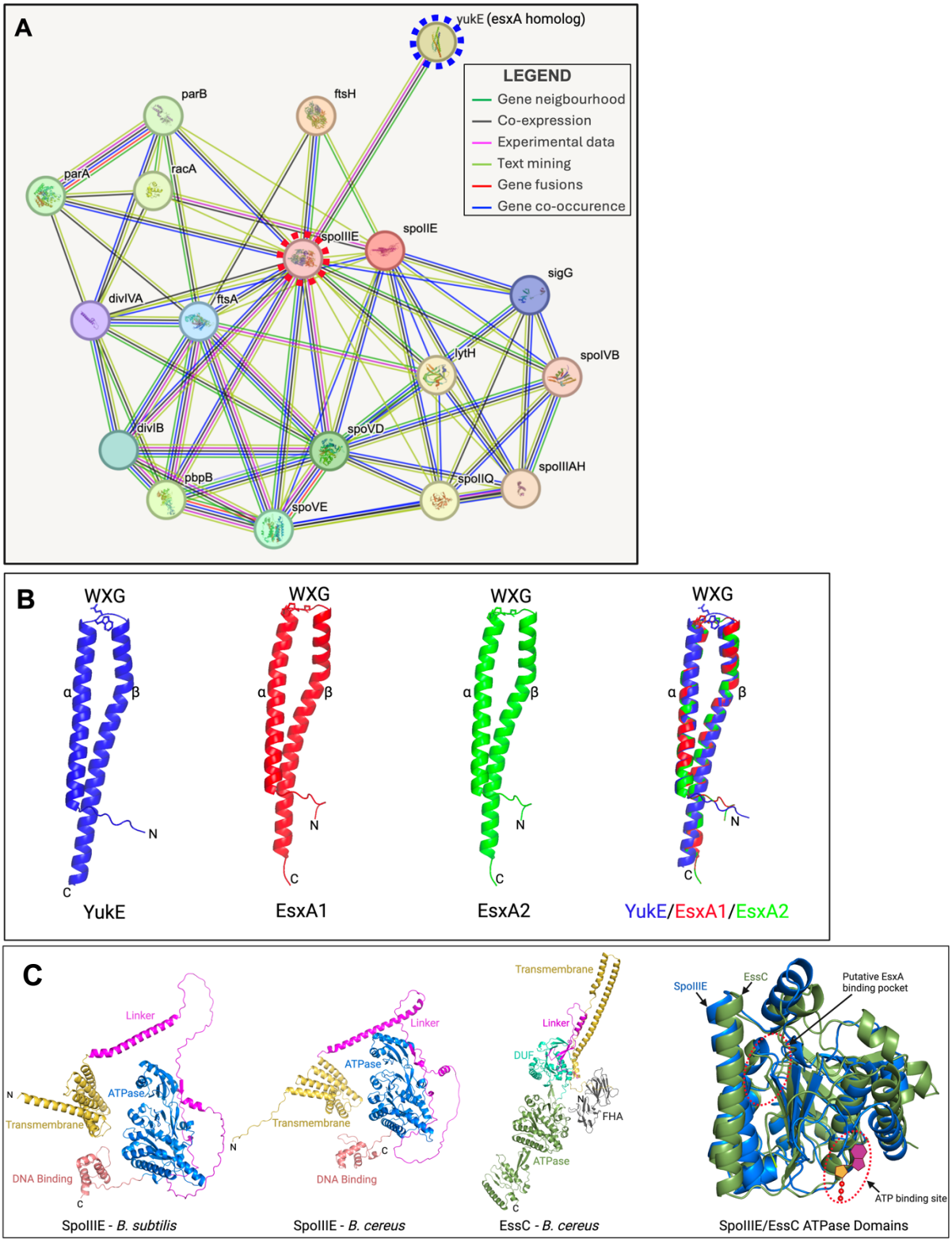

Figure 19. EsxA may be influencing sporulation via SpoIIIE.

A. String analysis of sporulation gene network for *B. subtilis* 168. The *yukE* (blue dotted circle), an *esxA* homologue, was predicted to have a direct link to SpoIIIE (red dotted circle), the DNA translocase during sporulation.

B. Structural comparison of WXG100 proteins from *B. subtilis* 168 (YukE) and *B. cereus* ATCC14579 (EsxA1 and EsxA2). YukE/EsxA1/EsxA2 shows the structural alignment of the three WXG100 proteins. The homology of the YukE to EsxA1 and EsxA2 is about 36 %, with 65% positives.

C. Molecular model structures of FtsK/SpoIIIE ATPase proteins with distinct domains are shown in different colours. SpoIIIE in *B. subtilis* and *B. cereus* are similar and nearly identical in the ATPase domain with 96% homology. Superimposition of the ATPase domains shows the putative binding pocket for EsxA on EssC and SpoIIIE in *B. cereus* and *B. subtilis*.

General conclusion

B. cereus and *B. anthracis* are Gram-positive, spore-forming bacteria of significant public health importance. These species and their strains have been defined based on their phenotypes and clinical and economic significance. *B. cereus* has long been a major cause of food poisoning, severe extra-intestinal infections and nosocomial infections in humans. In animals, *B. cereus* causes gangrenous mastitis, abortion and haemorrhagic disease, thus, it displays a variety of virulence mechanisms in multiple mammalian species. One of the mechanisms by which bacteria express their pathogenicity is specialized secretion systems, the T7SS for Gram-positive bacteria. However, the T7SS in *B. cereus* was previously uncharacterized. This study provided a detailed analysis of the T7SS in *B. cereus*, focusing on the role of its effector proteins.

In Chapter I, through genome and gene deletions analyses, the study identified a conserved T7SS cluster in *B. cereus* ATCC14579, containing essential genes such as *essA*, *esaA*, *essB*, *esaB*, and *essC*, in addition to two distinct *esxA* genes (*esxA1* and *esxA2*) and a toxin-associated LXG protein chaperone, *tigR*. Secretion of EsxA1 and EsxA2 was found to be dependent on a functional EssC. Comparative genomic analyses of *Bacillus* species and related strains demonstrated a variation in T7SS among the strains, particularly in clinical isolates of *B. cereus*, such as 30040 and B4264, and *B. anthracis,* which harbours additional virulence-related genes. The T7SSb-related genes in *B. anthracis* are not typically arranged but are scattered across the genome, including the pXO1 plasmid. Some of these genes make part of the TA clusters, thus linking T7SSb to the TA system. Additionally, *B. anthracis* T7SS loci include *sseB*, a gene that encodes a T3SS translocon protein. This variability suggests a potential role for T7SS diversity in niche adaptation and virulence across different environments or hosts.

In Chapter II, the study showed that deletion of both *esxA1* and *esxA2* led to a delayed and reduced sporulation rate, suggesting that EsxA proteins contribute to sporulation efficiency. Interestingly, sporulation defects observed in the *ΔesxA1ΔesxA2* mutant were not due to cell morphology changes but rather a decline in viable spore production despite normal growth and colony morphology. Furthermore, when complemented with either *esxA1* or *esxA2*, the mutant regained normal sporulation ability, underscoring the complementary functions of EsxA1 and EsxA2, respectively. This finding is clinically significant, as spores play a vital role in biofilm formation, resistance to disinfectants, and survival on hospital surfaces and equipment, which are challenging in infection control.

This study highlights the potential for targeting T7SS-dependent effectors, EsxA in this case, for antimicrobial development. As sporulation and biofilm formation are integral to *B. cereus* lifecycle and survival in hostile environments, inhibiting these processes could weaken the bacterium's resilience, potentially reducing its pathogenicity and resistance to disinfectants. The work also contributes to the broader understanding of T7SS diversity in Gram-positive bacteria. Given that the dormant spores of *B. cereus* and *B. anthracis* are the main infectious form of the bacteria, it suggests that T7SS-mediated adaptations could enable these pathogens of public health importance to thrive in both environmental and clinical settings. The results presented here indicate that the T7SS may operate beyond virulence but also in ecological resilience. The findings open avenues for further studies on molecular mechanisms that could shed light on how these secretion systems contribute to bacterial fitness and pathogenic potential.

Acknowledgements

I wish to express my cordial gratitude to my supervisors, Professor Hideaki Higashi, Assistant Professor Atmika Paudel, Senior Lecturer Yoshikazu Furuta, Associate Professor Tomoe Kitao at the Division of Infection and Immunity, International Institute for Zoonosis Control, Graduate School of Infectious Diseases, Hokkaido University for their support and guidance.

I also wish to thank Professor Bernard Mudenda Hang'ombe from the Microbiology Unit, School of Veterinary Medicine, University of Zambia, Professor Musso Munyeme from the Disease Control Unit, School of Veterinary Medicine, University of Zambia and Assistant Professor Misheck Shawa, Hokkaido University Center for Zoonosis Control in Zambia, International Institute for Zoonosis Control, Graduate School of Infectious Diseases, Hokkaido University/School of Veterinary Medicine, University of Zambia, for their kind support, mentorship and opportunity rendered to me to further my research.

I pay my gratitude to the World-leading Innovative and Smart Education (WISE) Office, Professor Motohiro Horiuchi, Department of Veterinary Hygiene, Hokkaido University, Ms. Junko Hayashi, Ms. Masaki Sato and Ms. Yoshioka Suzuka for their support.

I would like to acknowledge the professional support from Professor Ayato Takada, Division of Global Epidemiology, International Institute for Zoonosis Control, Graduate School of Infectious Diseases, Hokkaido University, Professor Junya Yamagishi, Division of Collaboration and Education, International Institute for Zoonosis Control, Graduate School of Infectious Diseases, Hokkaido University and Associate Professor Manabu Igarashi, Division of Global Epidemiology, International Institute for Zoonosis Control, Graduate School of Infectious Diseases, Hokkaido University.

I also thank past and present members of the Division of Infection and Immunity, Assistant Professor Tuvshinzaya Zorigt, Ms Tomoko Shimizu, Ms Misa Sugawara, Ms Mungusar Chuluun and Ms Ryo Oikawa for their support.

I also am grateful to my family and friends for their support and patience. Special recognition and appreciation go to Mr Japhet Chinyemba Kamboyi, Ms Mary Kalunguti, Late Mrs Mary Chabala Kamboyi, Ms Chloé Kamboyi, Ms Channah Likozhi Kamboyi, Mr Caius Kakoma Kamboyi and Mr Muchinka Benjamin Kamboyi for their unwavering support and enduring my absence from home.

Finally, I am grateful to the Japan International Cooperation Agency (JICA) for granting me the PhD scholarship and the Japan Initiative for Global Research Network on

Infectious Diseases (J-GRID), the Ministry of Education Culture, Sports, Science and Technology (MEXT) and the WISE Programme for their financial support during my training.

References

1. Cote CK, Heffron JD, Bozue JA, Welkos SL. *Bacillus anthracis* and Other *Bacillus* Species. Molecular Medical Microbiology. 2015, 1;1789–1844.
2. Priest FG, Barker M, Baillie LWJ, Holmes EC, Maiden MCJ. Population Structure and Evolution of the *Bacillus cereus* Group. J Bacteriol. 2004, 186(23):7959–7970.
3. RASKO D, ALTHERR M, HAN C, RAVEL J. Genomics of the *Bacillus cereus* group of organisms. FEMS Microbiol Rev. 2005, 29(2):303–329.
4. Liu Y, Lai Q, Göker M, Meier-Kolthoff JP, Wang M, Sun Y, et al. Genomic insights into the taxonomic status of the *Bacillus cereus* group. Sci Rep. 2015, 16;5(1):e14082.
5. Granum PE, Lund T. *Bacillus cereus* and its food poisoning toxins. FEMS Microbiol Lett. 2006, 17;157(2):223–228.
6. Ehling-Schulz M, Guinebretiere MH, MonthÃ¡n A, Berge O, Fricker M, Svensson B. Toxin gene profiling of enterotoxic and emetic *Bacillus cereus*. FEMS Microbiol Lett. 2006, 260(2):232–240.
7. Akamatsu R, Suzuki M, Okinaka K, Sasahara T, Yamane K, Suzuki S, et al. Novel sequence type in *Bacillus cereus* strains associated with nosocomial infections and bacteremia, Japan. Emerg Infect Dis. 2019, 25(5):883–890.
8. Ikram S, Heikal A, Finke S, Hofgaard A, Rehman Y, Sabri AN, et al. *Bacillus cereus* biofilm formation on central venous catheters of hospitalised cardiac patients. Biofouling. 2019, 35(2):204–216.
9. Savini Vincenzo. *Bacillus cereus* Disease in Animals. In: The Diverse Faces of *Bacillus cereus*. V. Academic Press, London UK. 2016, pp. 107–115.
10. Hussein MF. Endotoxicosis in Camels (Hemorrhagic Disease; Hemorrhagic Diathesis; *Bodus cereus* Intoxication). In: Infectious Diseases of Dromedary Camels. Springer, Cham, Switzerland. 2021. pp. 135–138.
11. Cheng L, Rao S, Poudyal S, Wang P, Chen S. Genotype and virulence gene analyses of *Bacillus cereus* group clinical isolates from the Chinese softshell turtle (*Pelodiscus sinensis*) in Taiwan. J Fish Dis. 2021, 44(10):1515–1529.
12. Tseng TT, Tyler BM, Setubal JC. Protein secretion systems in bacterial-host associations, and their description in the Gene Ontology. BMC Microbiol. 2009, 9;1(1):S2.
13. Grossman AS, Mauer TJ, Forest KT, Goodrich-Blair H. A Widespread Bacterial Secretion System with Diverse Substrates. mBio. 2021, 12(4):e0195621.

14. Arechaga I, Cascales E. Editorial: Bacterial Secretion Systems, Volume II. Front Microbiol. 2022, 13:917591.
15. Abdallah AM, Gey van Pittius NC, Champion PAD, Cox J, Luirink J, Vandenbroucke-Grauls CMJE, et al. Type VII secretion--mycobacteria show the way. Nat Rev Microbiol. 2007, 5(11):883–891.
16. Bunduc CM, Bitter W, Houben ENG. Structure and Function of the Mycobacterial Type VII Secretion Systems. Annu Rev Microbiol. 2020, 74(1):315–335.
17. Kneuper H, Cao ZP, Twomey KB, Zoltner M, Jäger F, Cargill JS, et al. Heterogeneity in *ess* transcriptional organization and variable contribution of the Ess/Type VII protein secretion system to virulence across closely related *Staphylococcus aureus* strains. Mol Microbiol. 2014, 93(5):928–943.
18. Mietrach N, Damián-Aparicio D, Mielich-Süss B, Lopez D, Geibel S. Substrate Interaction with the EssC Coupling Protein of the Type VIIb Secretion System. J Bacteriol. 2020, 202(7):e006646-19.
19. Simeone R, Bobard A, Lippmann J, Bitter W, Majlessi L, Brosch R, et al. Phagosomal rupture by *Mycobacterium tuberculosis* results in toxicity and host cell death. PLoS Pathog. 2012, 8(2):e1002507.
20. van der Wel N, Hava D, Houben D, Fluitsma D, van Zon M, Pierson J, et al. *M. tuberculosis* and *M. leprae* translocate from the phagolysosome to the cytosol in myeloid cells. Cell. 2007, 129(7):1287–1298.
21. Spencer BL, Tak U, Mendonça JC, Nagao PE, Niederweis M, Doran KS. A type VII secretion system in Group B *Streptococcus* mediates cytotoxicity and virulence. PLoS Pathog. 2021, 17(12):e1010121.
22. Bobrovskyy M, Chen X, Missiakas D. The Type 7b Secretion System of *S. aureus* and Its Role in Colonization and Systemic Infection. Infect Immun. 2023, 91(5):e0001523.
23. Burts ML, Williams WA, DeBord K, Missiakas DM. EsxA and EsxB are secreted by an ESAT-6-like system that is required for the pathogenesis of *Staphylococcus aureus* infections. Proceedings of the National Academy of Sciences. 2005, 102(4):1169–1174.
24. Warne B, Harkins CP, Harris SR, Vatsiou A, Stanley-Wall N, Parkhill J, et al. The Ess/Type VII secretion system of *Staphylococcus aureus* shows unexpected genetic diversity. BMC Genomics. 2016, 17(1):222.
25. Bobrovskyy M, Chen X, Missiakas D. The Type 7b Secretion System of *S. aureus* and Its Role in Colonization and Systemic Infection. Infect Immun. 2023, 91(5):e0001523.

26. Spencer BL, Tak U, Mendonça JC, Nagao PE, Niederweis M, Doran KS. A type VII secretion system in Group B *Streptococcus* mediates cytotoxicity and virulence. PLoS Pathog. 2021,17(12):e1010121.
27. Korea CG, Balsamo G, Pezzicoli A, Merakou C, Tavarini S, Bagnoli F, et al. Staphylococcal Esx Proteins Modulate Apoptosis and Release of Intracellular *Staphylococcus aureus* during Infection in Epithelial Cells. Infect Immun. 2014, 82(10):4144–4153.
28. Burts ML, DeDent AC, Missiakas DM. EsaC substrate for the ESAT-6 secretion pathway and its role in persistent infections of *Staphylococcus aureus*. Mol Microbiol. 2008, 69(3):736–746.
29. Bowran K, Palmer T. Extreme genetic diversity in the type VII secretion system of *Listeria monocytogenes* suggests a role in bacterial antagonism. Microbiology (N Y). 2021, 167(3):mic.0.001034.
30. Garrett SR, Higginson AB, Palmer T. Multiple variants of the type VII secretion system in Gram-positive bacteria. microLife. 2024, 5:uqae013.
31. Breijyeh Z, Karaman R. Design and Synthesis of Novel Antimicrobial Agents. Antibiotics. 2023, 12(3):628.
32. Rao C.V. S, De Waelheyns E, Economou A, Anné J. Antibiotic targeting of the bacterial secretory pathway. Biochimica et Biophysica Acta (BBA) - Molecular Cell Research. 2014, 1843(8):1762–1783.
33. Sheremet AB, Nesterenko LN, Zigangirova NA. The Type Three Secretion System of *Pseudomonas aeruginosa* as a Target for Development of Antivirulence Drugs. Molecular Genetics, Microbiology and Virology. 2020, 35(1):1–13.
34. McShan AC, De Guzman RN. The Bacterial Type III Secretion System as a Target for Developing New Antibiotics. Chem Biol Drug Des. 2015, 85(1):30–42.
35. Garufi G, Butler E, Missiakas D. ESAT-6-Like Protein Secretion in *Bacillus anthracis*. J Bacteriol. 2008, 190(21):7004–7011.
36. Philippot L, Griffiths BS, Langenheder S. Microbial Community Resilience across Ecosystems and Multiple Disturbances. Microbiology and Molecular Biology Reviews. 2021, 85(2):e00026-20.
37. Lamba S, Mundanda Muthappa D, Fanning S, Scannell AGM. Sporulation and Biofilms as Survival Mechanisms of *Bacillus* Species in Low-Moisture Food Production Environments. Foodborne Pathog Dis. 2022, 19(7):448–462.

38. Wood JP, Meyer KM, Kelly TJ, Choi YW, Rogers J V., Riggs KB, et al. Environmental Persistence of *Bacillus anthracis* and *Bacillus subtilis* Spores. PLoS One. 2015, 10(9):e0138083.
39. Marathe A, Zarazúa-Osorio B, Srivastava P, Fujita M. The master regulator for entry into sporulation in *Bacillus subtilis* becomes a mother cell-specific transcription factor for forespore engulfment. Mol Microbiol. 2023, 120(3):439–461.
40. Veening JW, Murray H, Errington J. A mechanism for cell cycle regulation of sporulation initiation in *Bacillus subtilis*. Genes Dev. 2009, 23(16):1959–1970.
41. Maphosa S, Moleleki LN, Motaung TE. Bacterial secretion system functions: evidence of interactions and downstream implications. Microbiology (N Y). 2023, 169(4):001326.
42. Filloux A. Bacterial protein secretion systems: Game of types. Microbiology (N Y). 2022, 168(5):mic.0.001193.
43. Gey Van Pittius NC, Gamieldien J, Hide W, Brown GD, Siezen RJ, Beyers AD. The ESAT-6 gene cluster of *Mycobacterium tuberculosis* and other high G+C Gram-positive bacteria. Genome Biol. 2001, 2(10):RESEARCH0044.
44. Zoltner M, Ng WMAV, Money JJ, Fyfe PK, Kneuper H, Palmer T, et al. EssC: domain structures inform on the elusive translocation channel in the Type VII secretion system. Biochemical Journal. 2016, 473(13):1941–1952.
45. Sysoeva TA, Zepeda-Rivera MA, Huppert LA, Burton BM. Dimer recognition and secretion by the ESX secretion system in *Bacillus subtilis*. Proceedings of the National Academy of Sciences. 2014, 111(21):7653–7658.
46. Renshaw PS, Lightbody KL, Veverka V, Muskett FW, Kelly G, Frenkiel TA, et al. Structure and function of the complex formed by the tuberculosis virulence factors CFP-10 and ESAT-6. EMBO J. 2005, 24(14):2491–2498.
47. Klein TA, Grebenc DW, Shah PY, McArthur OD, Dickson BH, Surette MG, et al. Dual Targeting Factors Are Required for LXG Toxin Export by the Bacterial Type VIIb Secretion System. mBio. 2022, 13(5):e0213722.
48. Cao Z, Casabona MG, Kneuper H, Chalmers JD, Palmer T. The type VII secretion system of *Staphylococcus aureus* secretes a nuclease toxin that targets competitor bacteria. Nat Microbiol. 2016, 2(1):16183.
49. Enosi Tuipulotu D, Mathur A, Ngo C, Man SM. *Bacillus cereus*: Epidemiology, Virulence Factors, and Host–Pathogen Interactions. Trends Microbiol. 2021, 29(5):458–471.

50. Tassinari M, Doan T, Bellinzoni M, Chabalier M, Ben-Assaya M, Martinez M, et al. The Antibacterial Type VII Secretion System of *Bacillus subtilis*: Structure and Interactions of the Pseudokinase YukC/EssB. mBio. 2022, 13(5):0013422.
51. Huppert LA, Ramsdell TL, Chase MR, Sarracino DA, Fortune SM, Burton BM. The ESX System in *Bacillus subtilis* Mediates Protein Secretion. PLoS One. 2014, 9(5):e96267.
52. Ivanova N, Sorokin A, Anderson I, Galleron N, Candelon B, Kapatral V, et al. Genome sequence of *Bacillus cereus* and comparative analysis with *Bacillus anthracis*. Nature. 2003, 423(6935):87–91.
53. Darling ACE, Mau B, Blattner FR, Perna NT. Mauve: multiple alignment of conserved genomic sequence with rearrangements. Genome Res. 2004, 14(7):1394–1403.
54. Guy L, Roat Kultima J, Andersson SGE. genoPlotR: comparative gene and genome visualization in R. Bioinformatics. 2010, 26(18):2334–2335.
55. Gibson DG, Young L, Chuang RY, Venter JC, Hutchison CA, Smith HO. Enzymatic assembly of DNA molecules up to several hundred kilobases. Nat Methods. 2009, 6(5):343–345.
56. Simon R, Priefer U, Pühler A. A Broad Host Range Mobilization System for In Vivo Genetic Engineering: Transposon Mutagenesis in Gram Negative Bacteria. Bio/Technology. 1983, 1(9):784–791.
57. Plaut RD, Stibitz S. Improvements to a Markerless Allelic Exchange System for *Bacillus anthracis*. PLoS One. 2015, 10(12):e0142758.
58. Chan QWT, Howes CG, Foster LJ. Quantitative Comparison of Caste Differences in Honeybee Hemolymph. Molecular & Cellular Proteomics. 2006, 5(12):2252–2262.
59. Deng W, Yu HB, de Hoog CL, Stoynov N, Li Y, Foster LJ, et al. Quantitative Proteomic Analysis of Type III Secretome of Enteropathogenic *Escherichia coli* Reveals an Expanded Effector Repertoire for Attaching/Effacing Bacterial Pathogens. Molecular & Cellular Proteomics. 2012, 11(9):692–709.
60. Qian C, Chen H, Johs A, Lu X, An J, Pierce EM, et al. Quantitative Proteomic Analysis of Biological Processes and Responses of the Bacterium *Desulfovibrio desulfuricans* ND132 upon Deletion of Its Mercury Methylation Genes. Proteomics. 2018, 18(17):1700479.
61. Kanehisa M. Linking databases and organisms: GenomeNet resources in Japan. Trends Biochem Sci. 1997, 22(11):442–444.

62. Altschul SF, Gish W, Miller W, Myers EW, Lipman DJ. Basic local alignment search tool. J Mol Biol. 1990, 215(3):403–410.
63. Waterhouse A, Bertoni M, Bienert S, Studer G, Tauriello G, Gumienny R, et al. SWISS-MODEL: homology modelling of protein structures and complexes. Nucleic Acids Res. 2018, 46(1):296–303.
64. PyMOL (TM). The PyMOL Molecular Graphics System. Schrödinger, LCC; 2024.
65. Ulhuq FR, Gomes MC, Duggan GM, Guo M, Mendonca C, Buchanan G, et al. A membrane-depolarizing toxin substrate of the *Staphylococcus aureus* type VII secretion system mediates intraspecies competition. Proceedings of the National Academy of Sciences. 2020, 117(34):20836–20847.
66. Kobayashi K. Diverse LXG toxin and antitoxin systems specifically mediate intraspecies competition in *Bacillus subtilis* biofilms. PLoS Genet. 2021, 17(7):e1009682.
67. Xie HX, Lu JF, Zhou Y, Yi J, Yu XJ, Leung KY, et al. Identification and Functional Characterization of the Novel *Edwardsiella tarda* Effector EseJ. Infect Immun. 2015, 83(4):1650–1660.
68. Yang Y, Wan C, Xu H, Wei H. Identification and characterization of OmpL as a potential vaccine candidate for immune-protection against salmonellosis in mice. Vaccine. 2013, 31(28):2930–2936.
69. Hood RD, Singh P, Hsu F, Güvener T, Carl MA, Trinidad RRS, et al. A Type VI Secretion System of *Pseudomonas aeruginosa* Targets a Toxin to Bacteria. Cell Host Microbe. 2010, 7(1):25–37.
70. Sana TG, Berni B, Bleves S. The T6SSs of *Pseudomonas aeruginosa* Strain PAO1 and Their Effectors: Beyond Bacterial-Cell Targeting. Front Cell Infect Microbiol. 2016, 6(61).
71. Poulsen C, Panjikar S, Holton SJ, Wilmanns M, Song YH. WXG100 Protein Superfamily Consists of Three Subfamilies and Exhibits an α-Helical C-Terminal Conserved Residue Pattern. PLoS One. 2014, 9(2):e89313.
72. Unnikrishnan M, Constantinidou C, Palmer T, Pallen MJ. The Enigmatic Esx Proteins: Looking Beyond Mycobacteria. Trends Microbiol. 2017, 25(3):192–204.
73. Bowman L, Palmer T. The Type VII Secretion System of *Staphylococcus*. Annu Rev Microbiol. 2021, 75(1):471–494.
74. Baptista C, Barreto HC, São-José C. High Levels of DegU-P Activate an Esat-6-Like Secretion System in *Bacillus subtilis*. PLoS One. 2013, 8(7):e67840.

75. Cheng AG, DeDent AC, Schneewind O, Missiakas D. A play in four acts: *Staphylococcus aureus abscess* formation. Trends Microbiol. 2011, 19(5):225–232.
76. Dodson RJ, Durkin AS, Rosovitz MJ, Rasko DA, Hoffmaster A, Ravel J, et al. Genome sequence of *Bacillus cereus* B4264. Vol. Direct sub, NCBI. Maryland; 2008. Available from: https://www.genome.jp/dbget-bin/www_bget?refseq:NC_011772 (Accessed June 2023)
77. Zhong W, Shou Y, Yoshida TM, Marrone BL. Differentiation of *Bacillus anthracis*, B. cereus, and *B. thuringiensis* by using pulsed-field gel electrophoresis. Appl Environ Microbiol. 2007, 73(10):3446–3449.
78. Wood TE, Howard SA, Förster A, Nolan LM, Manoli E, Bullen NP, et al. The *Pseudomonas aeruginosa* T6SS Delivers a Periplasmic Toxin that Disrupts Bacterial Cell Morphology. Cell Rep. 2019, 29(1):187-201.e7.
79. Nikolaus T, Deiwick J, Rappl C, Freeman JA, Schröder W, Miller SI, et al. SseBCD Proteins Are Secreted by the Type III Secretion System of *Salmonella* Pathogenicity Island 2 and Function as a Translocon. J Bacteriol. 2001, 183(20):6036–6045.
80. Das S, Howlader DR, Lu T, Whittier SK, Hu G, Sharma S, et al. Immunogenicity and protective efficacy of nanoparticle formulations of L-SseB against *Salmonella* infection. Front Immunol. 2023, 14:1208848.
81. Renshaw PS, Panagiotidou P, Whelan A, Gordon S V., Hewinson RG, Williamson RA, et al. Conclusive Evidence That the Major T-cell Antigens of the *Mycobacterium tuberculosis* Complex ESAT-6 and CFP-10 Form a Tight, 1:1 Complex and Characterization of the Structural Properties of ESAT-6, CFP-10, and the ESAT-6·CFP-10 Complex. Journal of Biological Chemistry. 2002, 277(24):21598–21603.
82. Casadevall A. Evolution of Intracellular Pathogens. Annu Rev Microbiol. 2008, 62(1):19–33.
83. Soni J, Sinha S, Pandey R. Understanding bacterial pathogenicity: a closer look at the journey of harmful microbes. Front Microbiol. 2024, 15:1370818.
84. Tran HR, Grebenc DW, Klein TA, Whitney JC. Bacterial type VII secretion: An important player in host-microbe and microbe-microbe interactions. Mol Microbiol. 2021, 115(3):478–489.
85. Sreejit G, Ahmed A, Parveen N, Jha V, Valluri VL, Ghosh S, et al. The ESAT-6 Protein of *Mycobacterium tuberculosis* Interacts with Beta-2-Microglobulin (β2M) Affecting Antigen Presentation Function of Macrophage. PLoS Pathog. 2014, 10(10):e1004446.

86. Jung BG, Wang X, Yi N, Ma J, Turner J, Samten B. Early Secreted Antigenic Target of 6-kDa of *Mycobacterium tuberculosis* Stimulates IL-6 Production by Macrophages through Activation of STAT3. Sci Rep. 2017, 7(1):40984.
87. Burts ML, Williams WA, DeBord K, Missiakas DM. EsxA and EsxB are secreted by an ESAT-6-like system that is required for the pathogenesis of *Staphylococcus aureus* infections. Proceedings of the National Academy of Sciences. 2005, 102(4):1169–1174.
88. Zhang Q, Wang D, Jiang G, Liu W, Deng Q, Li X, et al. EsxA membrane-permeabilizing activity plays a key role in mycobacterial cytosolic translocation and virulence: effects of single-residue mutations at glutamine 5. Sci Rep. 2016, 6(1):32618.
89. Bao Y, Wang L, Sun J. A Small Protein but with Diverse Roles: A Review of EsxA in *Mycobacterium*–Host Interaction. Cells. 2021, 10(7):1645.
90. Callahan B, Nguyen K, Collins A, Valdes K, Caplow M, Crossman DK, et al. Conservation of Structure and Protein-Protein Interactions Mediated by the Secreted Mycobacterial Proteins EsxA, EsxB, and EspA. J Bacteriol. 2010, 192(1):326–335.
91. Fyans JK, Bignell D, Loria R, Toth I, Palmer T. The ESX type VII secretion system modulates development, but not virulence, of the plant pathogen *Streptomyces scabies* . Mol Plant Pathol. 2013, 14(2):119–130.
92. Bottone EJ. *Bacillus cereus*, a volatile human pathogen. Clin Microbiol Rev. 2010, 23(2):382–398.
93. El-Arabi TF, Griffiths MW. *Bacillus cereus* In: Foodborne Infections and Intoxications. Elsevier, Amsterdam, Netherlands. 2013, pp. 401–407.
94. Majed R, Faille C, Kallassy M, Gohar M. *Bacillus cereus* Biofilms-Same, Only Different. Front Microbiol. 2016, 7:1054.
95. Shin JY, Lopez-Garrido J, Lee SH, Diaz-Celis C, Fleming T, Bustamante C, et al. Visualization and functional dissection of coaxial paired SpoIIIE channels across the sporulation septum. Elife. 2015, 4:e06474.
96. Wu LJ, Errington J. *Bacillus subtilis* spoIIIE Protein Required for DNA Segregation During Asymmetric Cell Division. Science (1979). 1994, 264(5158):572–575.
97. Sharp MD, Pogliano K. Role of Cell-Specific SpoIIIE Assembly in Polarity of DNA Transfer. Science (1979). 2002, 295(5552):137–139.
98. Fleming TC, Shin JY, Lee SH, Becker E, Huang KC, Bustamante C, et al. Dynamic SpoIIIE assembly mediates septal membrane fission during *Bacillus subtilis* sporulation. Genes Dev. 2010, 24(11):1160–1172.

99. Rosenberg OS, Dovala D, Li X, Connolly L, Bendebury A, Finer-Moore J, et al. Substrates Control Multimerization and Activation of the Multi-Domain ATPase Motor of Type VII Secretion. Cell. 2015, 161(3):501–512.
100. Fiche JB, Cattoni DI, Diekmann N, Langerak JM, Clerte C, Royer CA, et al. Recruitment, Assembly, and Molecular Architecture of the SpoIIIE DNA Pump Revealed by Superresolution Microscopy. PLoS Biol. 2013, 11(5):e1001557.
101. Chan H, Mohamed AMT, Grainge I, Rodrigues CDA. FtsK and SpoIIIE, coordinators of chromosome segregation and envelope remodeling in bacteria. Trends Microbiol. 2022, 30(5):480–494.
102. Huang Q, Zhang Z, Liu Q, Liu F, Liu Y, Zhang J, et al. SpoVG is an important regulator of sporulation and affects biofilm formation by regulating Spo0A transcription in *Bacillus cereus* 0–9. BMC Microbiol. 2021, 21(1):172.
103. Chen M, Lyu Y, Feng E, Zhu L, Pan C, Wang D, et al. SpoVG is Necessary for Sporulation in *Bacillus anthracis*. Microorganisms. 2020, 8(4):548.
104. Schulthess B, Bloes DA, Berger-Bächi B. Opposing roles of σB and σB-controlled SpoVG in the global regulation of esxA in *Staphylococcus aureus*. BMC Microbiol. 2012, 12(1):17.
105. Jutras BL, Chenail AM, Rowland CL, Carroll D, Miller MC, Bykowski T, et al. Eubacterial SpoVG Homologs Constitute a New Family of Site-Specific DNA-Binding Proteins. PLoS One. 2013, 8(6):e66683.
106. Nicholson WL, Setlow P, Harwood C, Cutting SM. Molecular biological methods for *Bacillus*. John Willey. 1990, p. 391–450.
107. Janes BK, Stibitz S. Routine markerless gene replacement in *Bacillus anthracis*. Infect Immun. 2006, 74(3):1949–1953.
108. Gao T, Foulston L, Chai Y, Wang Q, Losick R. Alternative modes of biofilm formation by plant-associated *Bacillus cereus*. Microbiologyopen. 2015, 4(3):452–464.
109. Furuta Y, Tsujinouchi M, Shawa M, Zorigt T, Miyajima Y, Paudel A, et al. Complete Genome Sequences of 24 Strains of *Bacillus cereus* Isolated from Nosocomial Infection and Bacteremia Cases in Japan. Microbiol Resour Announc. 2022, 11(4):e0120321.
110. Shemesh M, Chai Y. A Combination of Glycerol and Manganese Promotes Biofilm Formation in *Bacillus subtilis* via Histidine Kinase KinD Signaling. J Bacteriol. 2013, 195(12):2747–2754.

111. Yan F, Yu Y, Gozzi K, Chen Y, Guo J hua, Chai Y. Genome-Wide Investigation of Biofilm Formation in *Bacillus cereus*. Appl Environ Microbiol. 2017, 83(13):e00561-17.
112. Li L, Jin J, Hu H, Deveau IF, Foley SL, Chen H. Optimization of sporulation and purification methods for sporicidal efficacy assessment on *Bacillus* spores. J Ind Microbiol Biotechnol. 2022, 49(4):kuac014.
113. Nicholson WL, Schuerger AC. *Bacillus subtilis* Spore Survival and Expression of Germination-Induced Bioluminescence After Prolonged Incubation Under Simulated Mars Atmospheric Pressure and Composition: Implications for Planetary Protection and Lithopanspermia. Astrobiology. 2005, 5(4):536–544.
114. Oktari A, Supriatin Y, Kamal M, Syafrullah H. The Bacterial Endospore Stain on Schaeffer Fulton using Variation of Methylene Blue Solution. J Phys Conf Ser. 2017, 812:012066.
115. Spencer BL, Doran KS. Evolving understanding of the type VII secretion system in Gram-positive bacteria. PLoS Pathog. 2022, 18(7):e1010680.
116. Flint JL, Kowalski JC, Karnati PK, Derbyshire KM. The RD1 virulence locus of *Mycobacterium tuberculosis* regulates DNA transfer in *Mycobacterium smegmatis*. Proceedings of the National Academy of Sciences. 2004, 101(34):12598–12603.
117. Lin Y, Briandet R, Kovács ÁT. *Bacillus cereus* sensu lato biofilm formation and its ecological importance. Biofilm. 2022, 4:100070.
118. Lim ES, Baek SY, Oh T, Koo M, Lee JY, Kim HJ, et al. Strain variation in *Bacillus cereus* biofilms and their susceptibility to extracellular matrix-degrading enzymes. PLoS One. 2021, 16(6):e0245708.
119. Park E, Hussain MS, Elahi F, Hossain A, Oh DH. Role of *Bacillus cereus* biofilm formation behavior in virulence and pathogenic characteristics. J Food Saf. 2023, 43(6):e13088.
120. Baron C, Coombes B. Targeting Bacterial Secretion Systems: Benefits of Disarmament in the Microcosm. Infect Disord Drug Targets. 2007, 7(1):19–27.
121. Belete TM. Novel targets to develop new antibacterial agents and novel alternatives to antibacterial agents. Hum Microb J. 2019, 11:100052.
122. Akpe San Roman S, Facey PD, Fernandez-Martinez L, Rodriguez C, Vallin C, Del Sol R, et al. A heterodimer of EsxA and EsxB is involved in sporulation and is secreted by a type VII secretion system in *Streptomyces coelicolor*. Microbiology (N Y). 2010, 156(6):1719–1729.

123. Huang Y, Flint SH, Palmer JS. *Bacillus cereus* spores and toxins – The potential role of biofilms. Food Microbiol. 2020, 90:103493.
124. Wijman JGE, de Leeuw PPLA, Moezelaar R, Zwietering MH, Abee T. Air-Liquid Interface Biofilms of *Bacillus cereus*: Formation, Sporulation, and Dispersion. Appl Environ Microbiol. 2007, 73(5):1481–1488.
125. Szklarczyk D, Kirsch R, Koutrouli M, Nastou K, Mehryary F, Hachilif R, et al. The STRING database in 2023: protein–protein association networks and functional enrichment analyses for any sequenced genome of interest. Nucleic Acids Res. 2023, 51(1):638–646.
126. Wu LJ, Lewis PJ, Allmansberger R, Hauser PM, Errington J. A conjugation-like mechanism for prespore chromosome partitioning during sporulation in *Bacillus subtilis*. Genes Dev. 1995, 9(11):1316–1326.
127. Eijlander RT, de Jong A, Krawczyk AO, Holsappel S, Kuipers OP. SporeWeb: an interactive journey through the complete sporulation cycle of *Bacillus subtilis*. Nucleic Acids Res. 2014, 42(1):685–691.
128. Higgins D, Dworkin J. Recent progress in *Bacillus subtilis* sporulation. FEMS Microbiol Rev. 2012, 36(1):131–148.
129. Riley EP, Schwarz C, Derman AI, Lopez-Garrido J. Milestones in *Bacillus subtilis* sporulation research. Microbial Cell. 2021, 8(1):1–16.
130. Omony J, de Jong A, Krawczyk AO, Eijlander RT, Kuipers OP. Dynamic sporulation gene co-expression networks for *Bacillus subtilis* 168 and the food-borne isolate *Bacillus amyloliquefaciens*: a transcriptomic model. Microb Genom. 2018, 4(2):e000157.
131. Bobrovskyy M, Oh SY, Missiakas D. Contribution of the EssC ATPase to the assembly of the type 7b secretion system in *Staphylococcus aureus*. Journal of Biological Chemistry. 2022, 298(9):102318.